Univerisity of Crete

Master Thesis

Submitted to Department of Physics

Towards two-dimensional Gallium Nitride

Supervisor:

Nikolaos Pelekanos

Committee Members:

Eleftherios Iliopoulos

Georgios Deligeorgis

Christina Siaitanidou

Heraklion, Greece, July 2020

Abstract

In recent years, two-dimensional materials, exhibiting unique properties in comparison with their bulk counterparts, have become a new field of interest. Group III-nitride semiconductors have also attracted the interest of researchers in the last two decades for their widespread applications in electronics and optoelectronics. Recently, there have been some efforts in the literature towards the fabrication of two-dimensional GaN, which would be an advantageous system in terms of its large band-gap and increased quantum confinement. However, these efforts have encountered difficulties related to their limited thickness and lateral size control.

In this work, we explore a new method for the fabrication of free-standing GaN membranes with varying thickness of 30, 10 and 5nm, by applying the photo-electrochemical (PEC) etching technique on especially-prepared GaN heterostructrures grown by molecular beam epitaxy. The idea is based on the selective etching of a sacrificial InGaN layer leading to free-standing GaN membranes, placed on the top of the structures. In most of our PEC experiments, we observed enhanced vertical etching of the top GaN layer, in contrast to the much preferred lateral etching direction, we originally envisaged. This was mainly due to the deficient In-composition of the sacrificial layer, obliging us to excite much closer to the GaN gap, thus inducing vertical etching of the top GaN surface. We successfully transferred this vertically-etched nanostructured GaN on PDMS, but we did not succeed in transferring it further from PDMS onto SiO_2/Si templates, for optical and SEM observations. In addition, in the samples with 5 and 10nm thick top GaN layers, we observed vertical etching phenomena without any photo-excitation, leading us to the conclusion that the ultrathin top GaN layers should be protected during PEC etching procedure.

Acknowledgments

Firstly, I would like to express my deep appreciation and gratitude to my scientific supervisor Prof. Nikolaos Pelekanos for the excellent cooperation we had these years. I am really grateful for giving me the opportunity to do research and for trusting me with this project. His dedication and continuous and patient guidance has been solely responsible for completing this work.

In addition, I cannot express enough thanks to my committee, Prof. Eleftherios Iliopoulos and Dr. Georgios Deligeorgis, for their continuous support and encouragement.

I would also like to offer my special thanks to Dr.Eva Monroy of the CEA/Grenoble group in France for the fabrication of the high quality of III- nitride heterostructures.

Furthermore, I would like to thank various people in MRG for their valuable technical support and for their contribution to this project. I would like to express my special appreciation to Mrs Maria Androulidaki for her advice and assistance in optoelectronics lab as well as for helping me with the optical characterization of samples for this project. In addition, I would like to offer my special thanks to Mrs Katerina Tsagaraki for AFM, XRD and SEM measurements and for her great cooperation and assistance.

Moreover, it is my privilege to express my gratitude to my family for encouraging and supporting me these two last years in my decision for the Master Degree in "Photonics and Nanoelectronics".

Last but not least, I would like to thank my friends in MRG facilities for their moral support and their help in completing this project.

Contents

Abstract **2**

Acknowledgements **3**

1 Introduction **7**

1.1 Two-dimensional materials 7

1.2 III-nitrides semiconductors 10

1.3 Towards the limit of 2D III-nitrides 13

2 Experimental Techniques **19**

2.1 Photoelectrochemical etching technique 19

2.2 X-Ray Diffraction 22

2.3 Scanning Electron Microscopy 23

2.4 Photoluminescence 24

2.5 Atomic Force Microscopy 25

2.6 Transfer 26

3 Experiments on a First Set of Samples **28**

3.1 Introduction . . . 28

3.2 Structure . . . 28

3.3 Characterization of as-grown samples . . . 29

3.3.1 Photoluminescence and Reflectance . . . 30

3.3.2 Atomic Force Microscopy . . . 31

3.3.3 XRD measurements . . . 32

3.4 Design of MESAs . . . 35

3.5 Photoelectrochemical etching procedure . . . 36

3.6 Transfer . . . 43

3.7 Conclusions . . . 45

4 Experiments on a Second Set of Samples **47**

4.1 Introduction . . . 47

4.2 Structure . . . 47

4.3 Characterization of as grown samples . . . 48

4.3.1 Photoluminescence . . . 49

4.3.2 Atomic Force Microscopy . . . 50

4.3.3 XRD measurements . . . 50

4.4 Design of Mesas . . . 52

4.5 Photoelectrochemical Etching Procedure . . . 52

4.6 Transfer 60

4.7 Conclusions 67

Bibliography **69**

Chapter 1

Introduction

1.1 Two-dimensional materials

In the past decade, two-dimensional materials have become a new field of interest due to their remarkable properties in comparison to their bulk counterparts. 2D materials are crystalline structures that consist of a single layer of atoms. They are not only two-dimensional, but they are also referred as layered materials with strong covalent bonds in-plane, and relatively weak interlayer interactions due to out of plane Van deer Waals forces which play an important role in their internal cohesive properties.

In 2004, graphene, a single layer of graphite was first demonstrated by Andre Geim and Konstantin Novoselov [1]. It is a single layer of pure carbon, one atom thick, and it is bonded together in a hexagonal honeycomb lattice as shown on the left of fig.1.1. It consists of two atoms A and B with a_1, a_2 basis vectors, respectively. On the right of Fig.1.1 the Brillouin zone of graphene is depicted.

What makes graphene so unique is the K and K' points at the corners of the hexagonal Brillouin zone (1.2), which are called Dirac points. Dirac points are so special thanks to the linear energy dispersion in contrast to most conventional metals and semiconductors. Due to this linearity, the carriers are described as mass-less particles following a Dirac-like equation. Additionally, the Fermi level in intrinsic graphene lies exactly at the Dirac points.

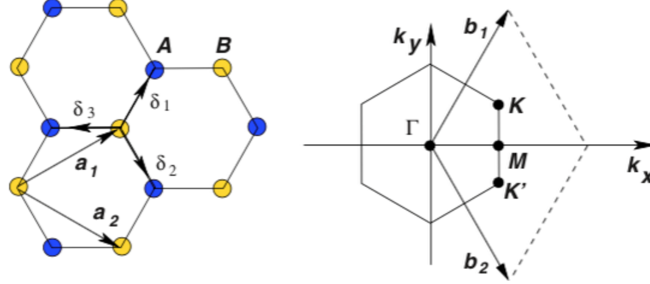

Figure 1.1: Schematic depicts the honeycomb lattice and Brillouin zone of graphene.[2]

Graphene fascinated the researchers due to its intriguing properties such as high thermal and electrical conductivity, mechanical strength, excellent optical transmittance etc., which make it a potential candidate for various applications. However, due to its zero-gap at the Dirac point, there are limitations on the applications that it can be used(e.g. MOSFET transistors cannot be switched-off).

The birth of graphene has opened new horizons to the research of other 2D materials with similar properties. During the last years, a new generation of other layered materials such as hexagonal Boron Nitride (h-BN), Transition Metals Dichalgogenides, Phosphorene, Xenes have been studied exhibiting interesting physical and chemical properties. Nowadays, a third generation of two dimensional non-layered materials is considered, referring to few-atom-thick layers, such as the 2D III-nitrides.

As previously mentioned, what fascinates the research community about 2D materials is their unique properties in contrast to their bulk counterparts. The nanomaterials change as a function of their size. Quantum confinement effects take place related to

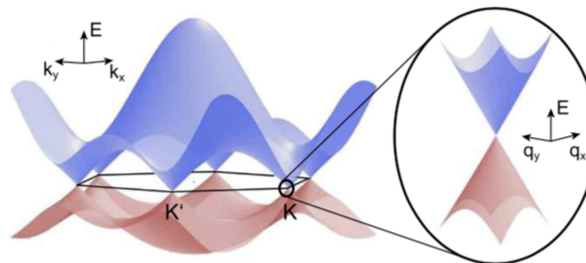

Figure 1.2: Electronic Dispersion of graphene and zoom in at K Dirac point.[3]

the spatial confinement of electrons in ultrathin materials, unlike their free motion inside bulk materials. The effect of spatial confinement varies from one material to another due to their different structure and composition. Excitons are electron-hole pairs which interact by the Coulomb potential. Their Bohr radius is an important length scale which represents their spatial extent typically over a few nanometers. When the particle size becomes lower than the Bohr radius the quantum confinement causes the reduction of the dielectric screening between electrons and holes. This intensifies on the Coulomb interactions, as more strongly bound excitons are found. As a result of quantum confinement, we have the increase of exciton energy and the blue-shift of the bandgap. In addition to this, it is important to mention that due to quantum confinement the whole band structure is strongly modified leading to unique optical and electronic properties. For example, monolayer MoS_2 not only exhibits an increase to its energies, but also the change of its bandgap from indirect to direct(Fig.1.3). Moreover, the large ratio of surface area to volume makes them more sensitive to external changes, which in turn renders them potential candidates for sensors. Last but not least, their layered structure with strong covalent bonds in-plane and ultrathin thickness makes them mechanically strong materials with optical transparency and great flexibility. Furthermore, the weak out of plane Van der Waals leads to "independence" from substrates, which plays an important role in forming heterostrucrures [4].

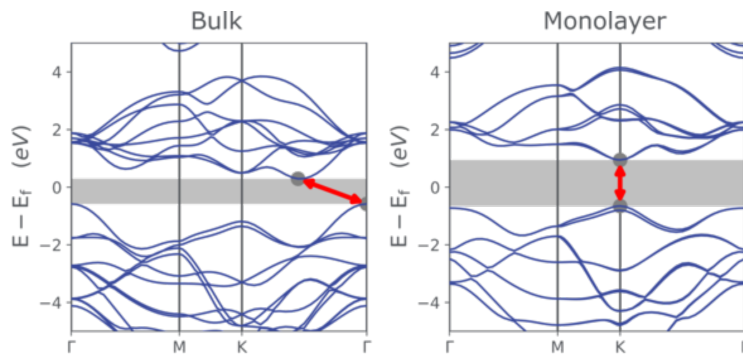

Figure 1.3: Schematic showing the increase of the energy and the change of bandgap nature from bulk to monolayer MoS_2 [5]

1.2 III-nitrides semiconductors

Group III-nitrides semiconductors have aroused the interest of researchers due to their remarkable properties. Group III-nitrides (AlN, GaN, InN) and their alloys (AlGaN, InGaN) have a wide direct bandgap which covers the electromagnetic spectrum from infrared to deep ultraviolet. Not only their tunable direct bandgap but also a bunch of other properties such as high thermal conductivity, high voltage breakdown, thermal stability etc. renders them as suitable materials for electronic and optoelectronic applications.

III-nitrides are able to crystallize in two main structures: cubic zinc blende which is thermodynamically metastable and hexagonal wurtzite which is thermodynamically stable. The wurtzite structure appertains to $P6_3mc$ group and it can be described by two different atoms which form a sublattice, HCP- type (hexagonal close-packed), along the c-axis. It contains 6 atoms in the hexagonal unit cell with a biatomic AaBbAa... stacking sequence. It can be characterized by the a-constant of the hexagon and the c-constant which is the height of the hexagonal prism. In addition, there is ionic bond between the anion-cation atoms which create a unit cell of a tetrahedron. The bond length between them is described by an internal parameter u along the c-axis (1.4).

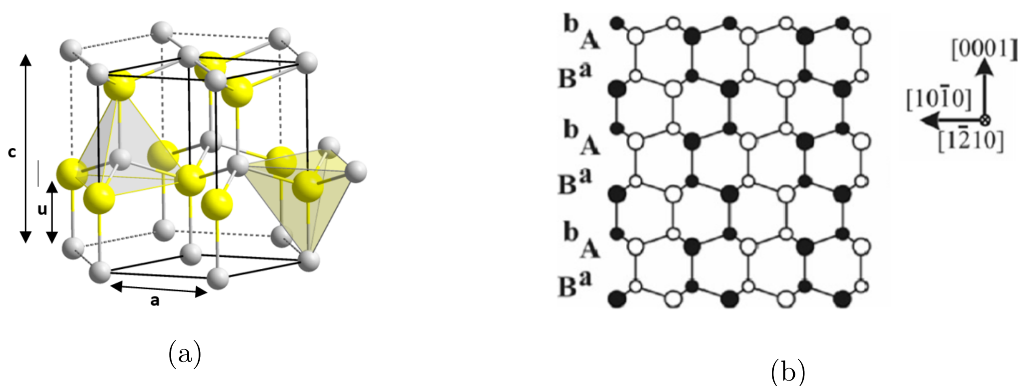

(a)

(b)

Figure 1.4: (a)A representation of wurtzite structure[6], (b) The BaAb stacking sequence on [0001] direction.

Some of their structural and physical properties of III-nitrides are shown in table1.1. In accordance to this, both gallium nitride (GaN) and aluminum nitride (AlN)

have a wide direct bandgap which makes them great candidates for optoelectronic applications. They can also synthesize alloys ($Al_xGa_{1-x}N$) and combine their properties leading to a variety of semiconductors. Additionally, indium nitride (InN) presents a low bandgap energy which makes it interesting for mid-infrared devices. However, its large lattice mismatch compared to GaN and the difficulty to control its residual doping have made it difficult so far to exploit InGaN for mid-infrared applications. Nevertheless, its alloys in combination with GaN and AlN are mainly used in applications. In this work, we use $In_xGa_{1-x}N$ with x between 10% and 20% as a sacrificial layer for the PEC etching technique.

	GaN	AlN	InN
Energy gap at 300(K)	3.437	6.00	1.89
Lattice constants a (Å)	3.189	3.112	3.545
Lattice constants c (Å)	5.185	4.982	3.703
Thermal expansion Δa/a (1/K)	$5.59x10^{-6}$	$4.2x10^{-6}$	$3.8x10^{-6}$
Thermal expansion Δc/c (1/K)	$3.17x10^{-6}$	$5.3x10^{-6}$	$2.9x10^{-6}$

Table 1.1: Material properties of group III-nitrides.[7]

The wurtzite structure is non-centrosymmetric which means that it lacks the inversion symmetry along the c-plane. However, this feature provides properties such as piezoelectricity and spontaneous polarization as well as different surface properties depending on whether the surface terminates on nitrogen atoms or metal atoms (Ga, In, Al). In the case of GaN, the crystal could be either Ga-faced or N-faced as shown in the figure 1.5.

The result of this uniaxial anisotropy is the change of the polarization charge. As the electrostatic interaction between anion (N^{3-}) and cation atom (Ga^{3+}) is large enough to reduce their interatomic distance, inducing spontaneous polarization (P_{sp}) with high concentration of bound charges at the interfaces. In addition, in III-V heterostructures, piezoelectricity polarization appears as an effect of strain. When a strain field is applied in these piezoelectric materials, electric charges appear on their surfaces. There are two types of strain, tensile and compressive, that depends on the different lattice constants of materials and thermal mismatch. More precisely, when AlGaN is grown on Ga-faced

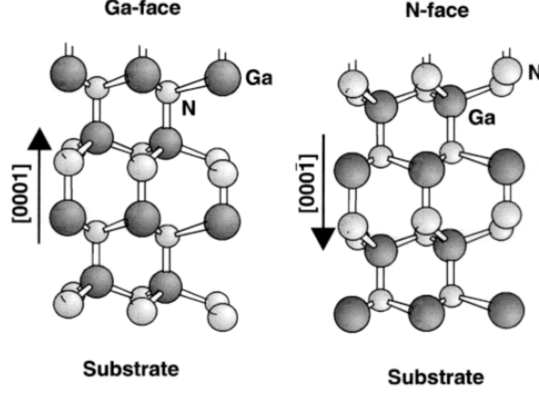

Figure 1.5: Ga-face and N-face polarity depending on the orientation of crystal growth[8].

GaN, tensile strain develops in AlGaN whereas in the case of InGaN the strain is compressive (1.6). In summary, the total polarization field of these structures is a result of the contribution of spontaneous (P_{sp}) and piezoelectric (P_p) polarizations.

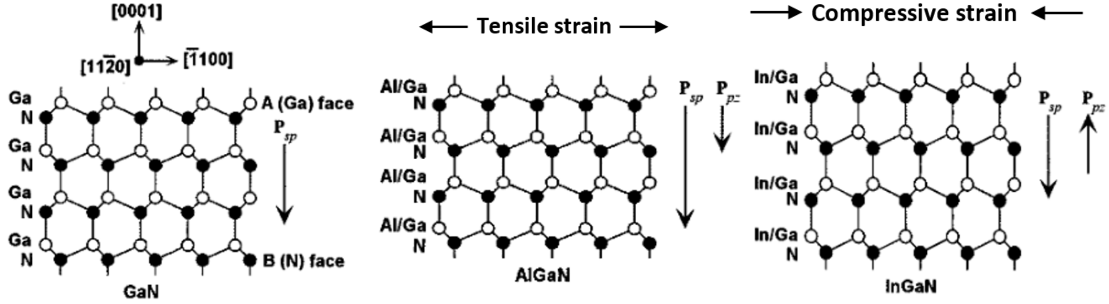

Figure 1.6: Crystal structure, spontaneous and piezoelectric polarization for (a) GaN, (b)AlGaN on GaN and (c) InGaN on GaN [9].

As mentioned earlier, nitride alloys have a great interest since by varying their content (x) of aluminum in $Al_xGa_{1-x}N$ and indium in $In_xGa_{1-x}N$, we get alloys that emit in a wide spectral range. By varying the relative concentrations of cations, it is feasible to fabricate semiconductors with different lattice constants and energy gaps. According to Vegard's model [10], the empirical relation for the bandgap of alloys is given by eq.1.1:

$$E_{g,AlGaN/InGaN}(x) = xE_{g,Al/InGaN} + (1-x)E_{g,GaN} - bx(1-x) \tag{1.1}$$

where the parameters b, for AlGaN b_{AlGaN}= 0.71eV and for InGaN b_{InGaN}= 1.7eV, are called parabolic bowing factors due to the parabolic dependence of the bandgap energy versus concentration. As regards to the a and c constants for the hexagonal structure, the relations of them versus the concentrations are, taken by Liou et al. :

$$a(x) = xa_{Al/InN} + (1-x)a_{GaN} - \delta_a x(1-x) \tag{1.2}$$

$$c(x) = xc_{Al/InN} + (1-x)c_{GaN} - \delta_c x(1-x) \tag{1.3}$$

where δ_a, δ_c are deviation bowing parameters for a and c constants respectively.

1.3 Towards the limit of 2D III-nitrides

Group III-nitrides have attracted the interest of researchers for many years and many applications have been developed based on them and their alloys. In spite of their great impact in blue-green optoelectronics, two dimensional III-nitrides semiconductors are still an unexplored field due to their difficulty to fabricate. However, over the last few years, theoretical studies have been made in order to estimate the properties of a few atomic layer-thick nitride semiconductors. It is predicted that there are two types of stable hexagonal structures, the planar and the buckled, depending on whether the unsaturated dangling bonds on the surface are passivated properly by using pseudo-hydrogen atoms (buckled structure) or not (planar structure)(fig.1.7). An ab initio hybrid density functional theory (DFT) has given calculations of the dissociation binding energy and bandgap energy due to quantum confinement. In fig.1.7a, is shown the binding energy for both of these structures on the basis of the number of atomic layers for the freestanding III-nitrides (AlN, GaN, InN). The comparison shows that the buckled structure is more thermodynamically stable, considering the more larger binding energy. In addition to this, in fig.1.7b the energy gap as a function of in-plane lattice parameter shows the blue shifted energy of the monolayer buckled structure of group III- nitrides in comparison with their bulk counterparts as well as, in the inset, where the energy gap dependence on the number of atomic layers is depicted.

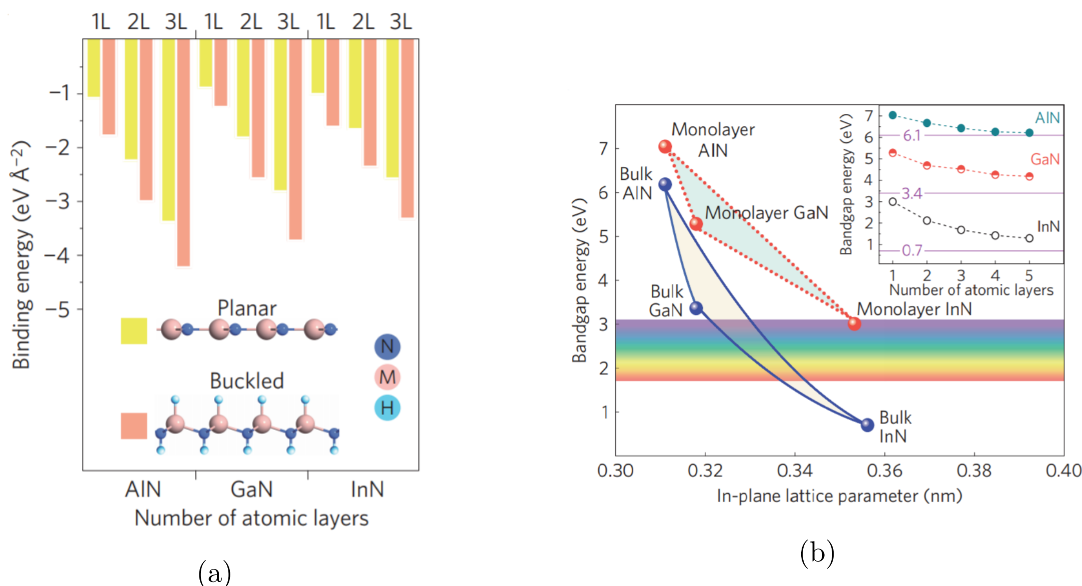

Figure 1.7: DFT calculations of (a) the binding energy of freestanding planar and buckled 2D nitrides as a function of the number of atomic layers and (b) the bandgap energy versus in-plane parameter lattice for the group III-nitrides.

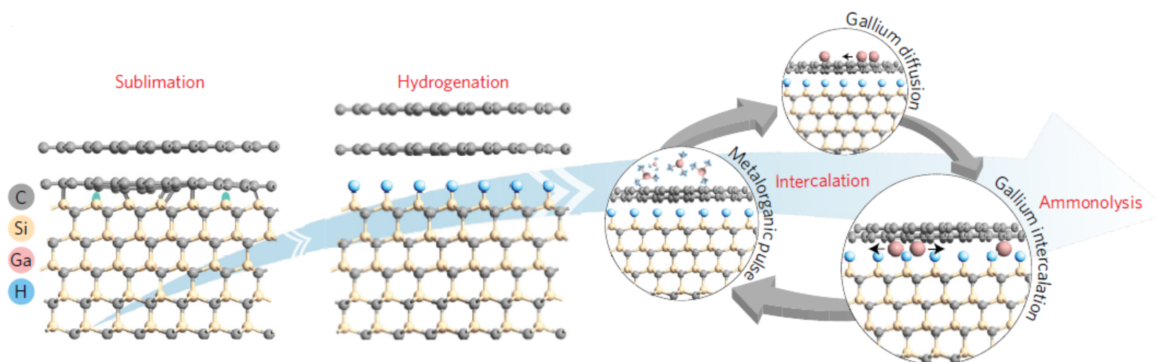

Figure 1.8: A schematic of the MEEG process

GaN has always been a great candidate for electronics and optoelectronics based on its intriguing characteristics, thus 2D GaN attracts immediately the interest of researchers. Balushi et al. demonstrated, for the first time, the synthesis of 2D GaN via migration-enhanced encapsulated growth technique (MEEG) [11]. In figure 1.8 the steps for the formation of 2D GaN is shown.

A SiC(0001) substrate was used as a template for the growth of 2D GaN. The first

step of the process starts with the sublimation of silicon and the formation of a buffer-layer of graphene. Hydrogenation reaction, in turn, takes place in order to passivate the unsaturated bonds of the surfaces between graphene buffer layer and SiC having as a result the formation of an additional quasi-freestanding epitaxial layer of graphene (QFEG). The next step refers to the intercalation of gallium adatoms between the substrate and the bi-layer of graphene by using trimethylgallium as a precursor. The intercalation is facilitated by the networks of wrinkles and defects of graphene (fig.1.9) and this is demonstrated conclusively by the fact that the growth of 2D GaN is preferential near grain boundaries and 3D islands of GaN, which formed where Ga-droplets had originally nucleated (fig.1.9b). Finally, ammonolysis comes to pass for the formation of 2D GaN. A buckled structure of 2D GaN with R3m symmetry (with st oichiometry GaN_x) is formed via MEEG as shown in fig.1.9c .

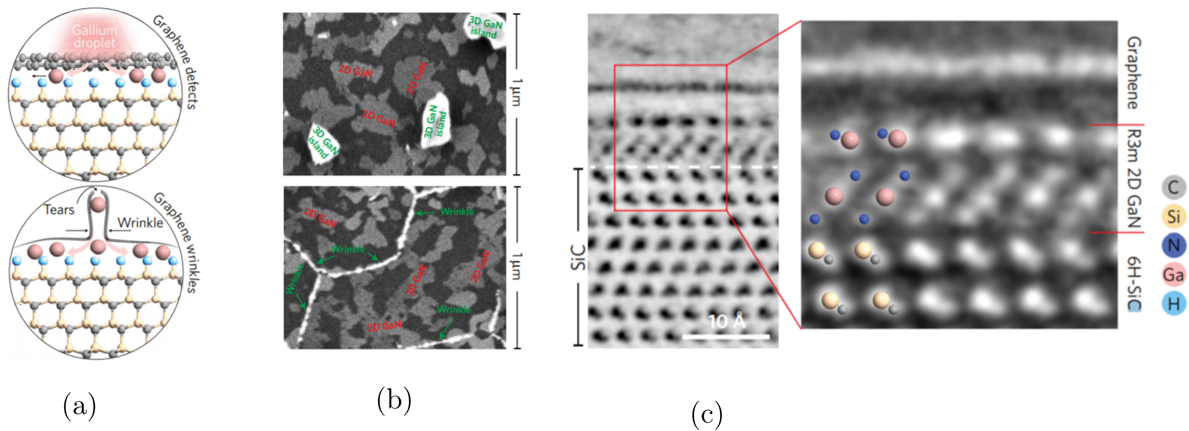

Figure 1.9: (a)Schematic for the intercalation pathways of gallium through defects and wrinkles of graphene, (b) A SEM image of the 2D GaN formation near 3D GaN islands and wrinkles (c)Annular bright-field (ABF) images resolving the atomic heterostructure.

The role of graphene as a capping layer is shown in fig.1.10. 3D islands formed on SiC(0001) without graphene capping (fig.1.10a) whereas there is a patchwork of 2D GaN when graphene was utilized (fig.1.10b). In addition, graphene had also an impact on the termination of GaN's growth. The thick GaN without graphene capping layer is gallium polar (fig.1.10d) whereas the 2D GaN interfacing graphene is nitrogen polar (fig. 1.10c). This is also evident by the formation of thicker layers of GaN (>5nm) which have the same surface termination as observed in 2D GaN.

After the synthesis of 2D GaN, absorbance and reflectance measurements were carried out showing a blue-shift of the energy bandgap (fig.1.11), in good agreement with the theoretical calculations they performed.

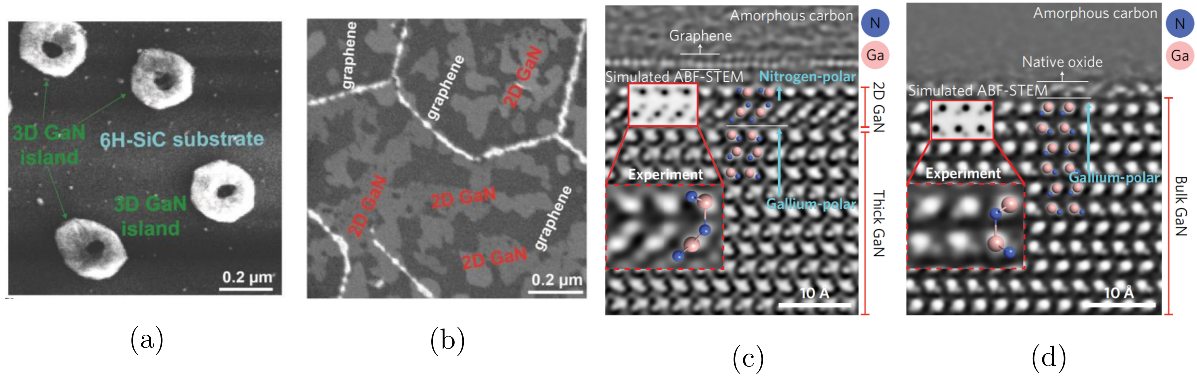

Figure 1.10: (a) SEM showing the formation of 3D GaN islands grown on 6H-SiC substrate and (b) 2D GaN grown when graphene was utilized, ABF-STEM images showing the inversion of surface termination from nitrogen-polar with graphene capping (c) to gallium-polar without graphene capping (d).

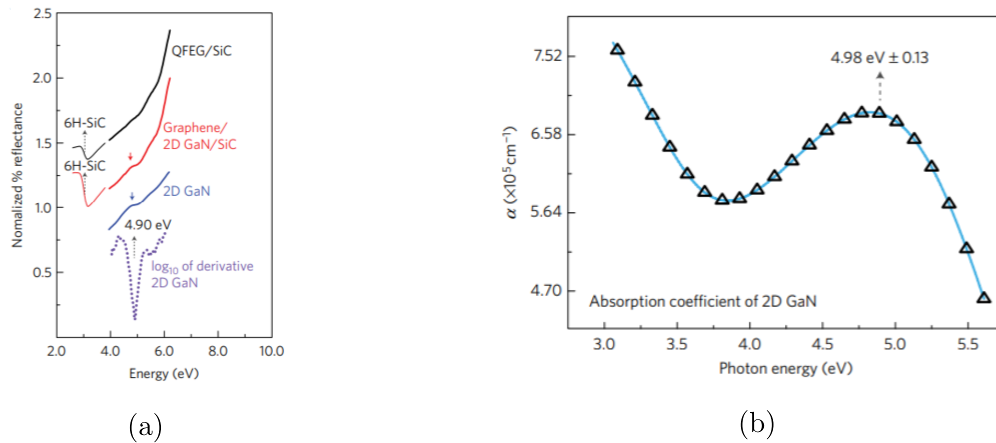

Figure 1.11: (a) UV-Vis reflectance measurements showing a transition at 4.90eV (b) The absorption coefficient (α) collected via UV-Vis spectroscopic ellipsometry predicting a direct energy gap of 2D GaN at 4.98 eV.

Recently, Fu et al. demonstrated another method for the synthesis of 2D GaN layers on Liquid Metals by a Surface Confined Nitridation Reaction (SCNR) via chemical vapor deposition (CVD) [12]. The SCNR procedure is shown in fig.1.12. Firstly, a W foil with a gallium pellet on its surface is placed in zone 2 and is heated up to 1080°

C. As the W's surface tension is far larger than Ga's, this results in the formation of a Ga/Ga-W interface region which consists of an ultrathin Ga layer and a subsurface Ga-W solid solution. Secondly, SCNR takes place using urea as a nitrogen source. The urea precursors are moved into zone 1 and nitridation reaction occurs mainly on the atomic Ga layer.The confined growth of 2D GaN is controlled by the stronger nitridation ability of W atoms which are held at Ga/Ga-W interface and prevent the thickening. The result of SCNR on liquid metals is the formation of micron-sized 2D GaN of different random thicknesses.

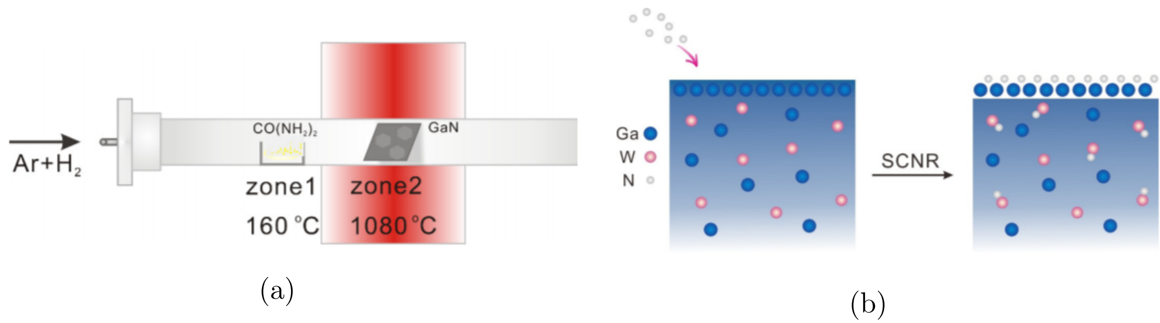

Figure 1.12: Schematic showing (a) the CVD procedure and (b) the SCNR for the growth of 2D GaN single crystals.

Measurements on the as-obtained 2D GaN were carried out in order to investigate their properties. They characterized the morphology and structure of the as-grown samples and they also investigated their optoelectronic properties. They report a blue-shifting PL peak with decreasing thickness (fig.1.13a,1.13b) as well as a red-shifted, strong and symmetric Raman peak (fig.1.13c). In addition to this, they constructed a Field Effect Transistor (FET) device in order to measure the mobility and on/off ratio of the 2D crystal (fig.1.13d-1.13f) .

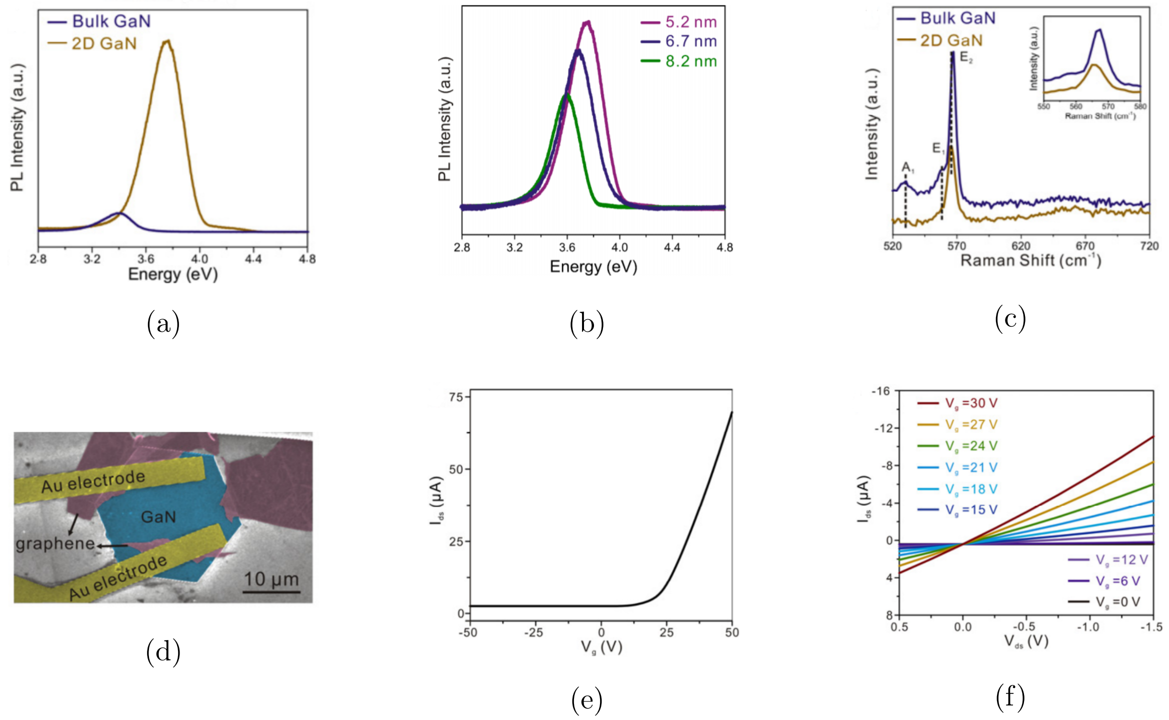

Figure 1.13: (a) PL spectra of a 5.2nm-thick GaN and bulk GaN, (b) PL specta of different thicknesses of 2D GaN, (c) Raman spectra of a 5.2nm 2D GaN and bulk GaN, (d) Schematic of 2D GaN FET, (e) I_{ds}-V_g characteristic curve at V_{ds}=1V, (f) I_{ds}-V_{ds} characteristic curvres.

Chapter 2

Experimental Techniques

2.1 Photoelectrochemical etching technique

PEC is a photoelectrochemical etching technique that was first developed by Minsky et al. on GaN films [13]. This technique is associated with rapid etch rates, lateral and bandgap etching selectivity under photo-enhanced electrons and holes in the semiconductors. In this work, we employ the PEC method for fabricating ultrathin GaN membranes using InGaN as a sacrificial layer for PEC.

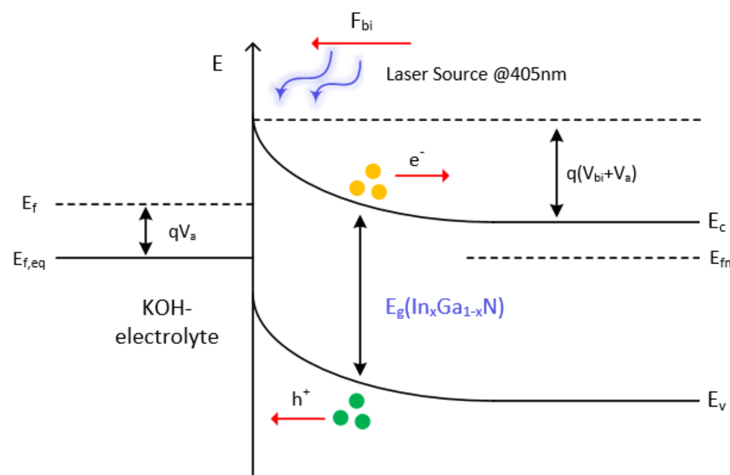

Figure 2.1: An illustration of the energy band diagram for an n-type InGaN semiconductor in contact with electrolyte under applied bias V$_a$ and illumination.

During the selective etching of InGaN a number of photoelectrochemical reactions take place:

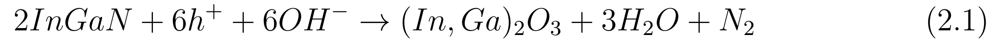

$$2InGaN + 6h^{+} + 6OH^{-} \rightarrow (In, Ga)_2O_3 + 3H_2O + N_2 \quad (2.1)$$

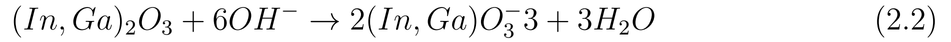

$$(In, Ga)_2O_3 + 6OH^{-} \rightarrow 2(In, Ga)O_3^{-}3 + 3H_2O \quad (2.2)$$

By using a UV laser diode, with energy greater than InGaN's bandgap, the photo-generated h^{+}'s move towards the InGaN/electrolyte interface. Once the hole accumulation occurs, the oxidation procedure of InGaN starts as InGaN reacts with the OH^{-} ions from the KOH solution and the holes at the surface (eq.2.1). The produced InGaN oxides react in turn with OH^{-} resulting in a further dissolution process (eq.2.2). In order to ensure the accumulation of the holes at the interface, a reverse voltage is applied (fig.2.1).

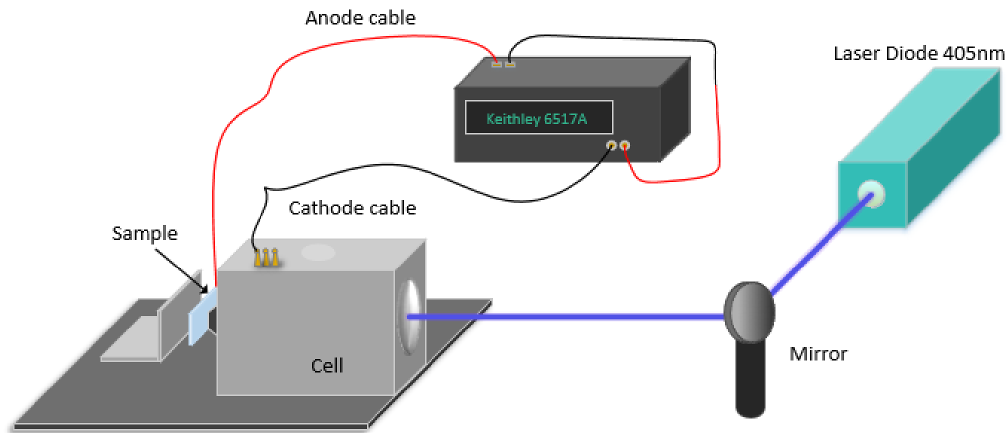

Figure 2.2: Schematic depicts the PEC set up.

In fig. 2.2 is depicted our PEC set up. A laser diode of 405nm is used which is especially selected as our excitation source. As InGaN is our sacrificial layer, the light

source has a photon energy greater than the InGaN's bandgap but less than AlGaN's and GaN's. In our case the InGaN etching is "lateral" as only the lateral sides are exposed to the electrolyte (Fig.2.3a). The beam is directed by a mirror to the electrochemical cell where the electrolyte KOH solution is placed. The beam goes through the cell and ends up to a $\sim 0.0078cm^2$ pinhole. At the end of this path, the sample is fitted vertically to the laser beam in contact with the pinhole and the electrolyte. The diameter of the pinhole is large enough so that the wetted-illuminated area on the sample contains a large number of mesas. As a consequence, the etching procedure is done simultaneously on all wetted mesas. An indium contact on the surface of the sample acts as an anode and a platinum electrode inside the cell as a cathode, which are connected to a Keithley 6517A power supply, controlled by a computer via an Agilent GPIB cable. By using the Agilent VEE software, it is possible to set the desired voltage and record the output current versus time during the PEC etching. This plays a major role in our experiments, as this set of measurements, enables the understanding of any deviations from the ideal curve (fig.2.3b).

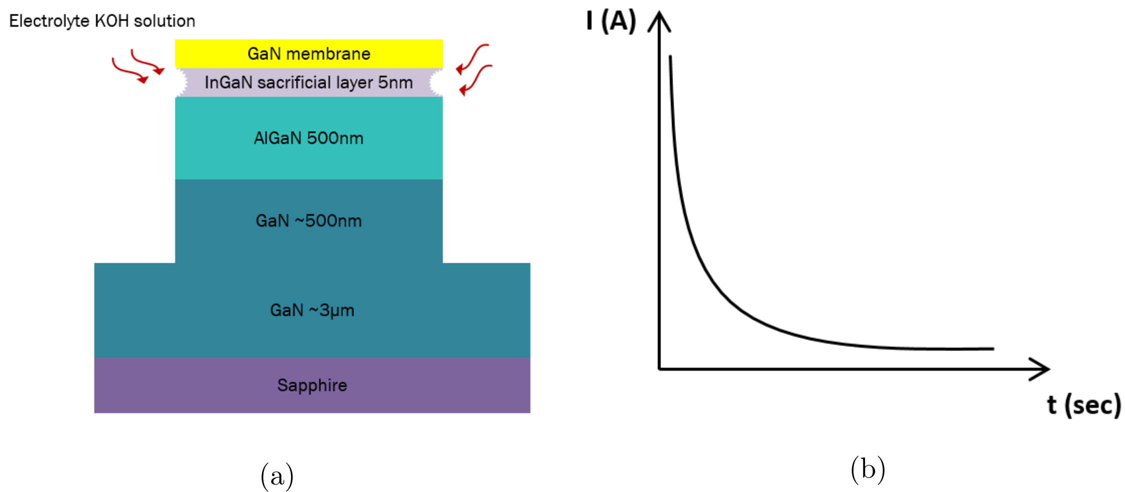

(a) (b)

Figure 2.3: Schematic depicts (a) the lateral PEC etching of our structures and (b) the characteristic ideal I-t curve during the PEC etching technique.

2.2 X-Ray Diffraction

X-ray Diffraction (XRD) is a technique that provides information about the crystalline structure of materials. An incident X-ray beam is diffracted at specific angles and by measuring the intensities from each set of lattice planes, a crystallographer can determine the atomic arrangement within the lattice planes [14].

X-rays consist of high energy photons with wavelength λ which is comparable with the interatomic distance in a crystal. When X-rays encounter these regularly spaced particles inside the crystal, diffraction occurs[15]. The atoms scatter the incident X-ray beam in all directions and the intensity of the electromagnetic wave depends on the interference pattern. Not all X-rays appear because of the destructive (out-of phase waves). The intensity of the diffracted beam depends on the angle between the diffracted beam and the solid. The relationship is given by Bragg's law.

Bragg's law:

Constructive interference occurs between two electromagnetic waves with the same phase. In figure 2.4, the difference between the 1' and 2' diffracted waves should be exactly one (or more) wavelengths. The path difference between the two waves is |SQ|+|QT|, which is equal to $2d_{dhkl}sin(\theta)$, where h,k,l are the Miller indices (Fig.2.4) [16].

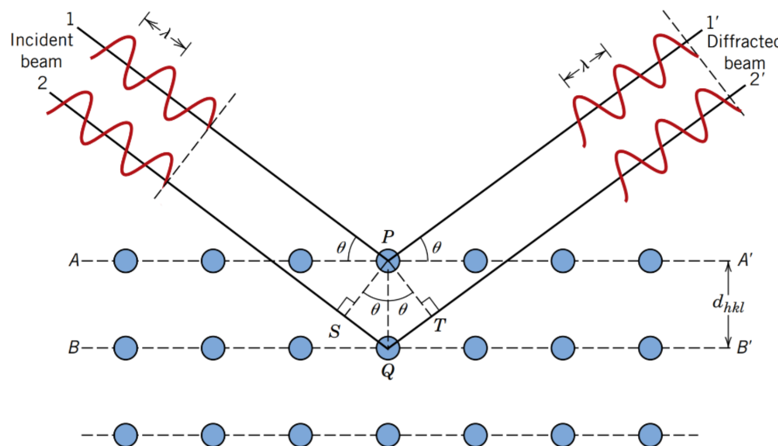

Figure 2.4: Diffraction of X-rays by atomic planes.

This results in the Bragg's law:

$$n\lambda = 2d_{hkl}sin(\theta) \tag{2.3}$$

2.3 Scanning Electron Microscopy

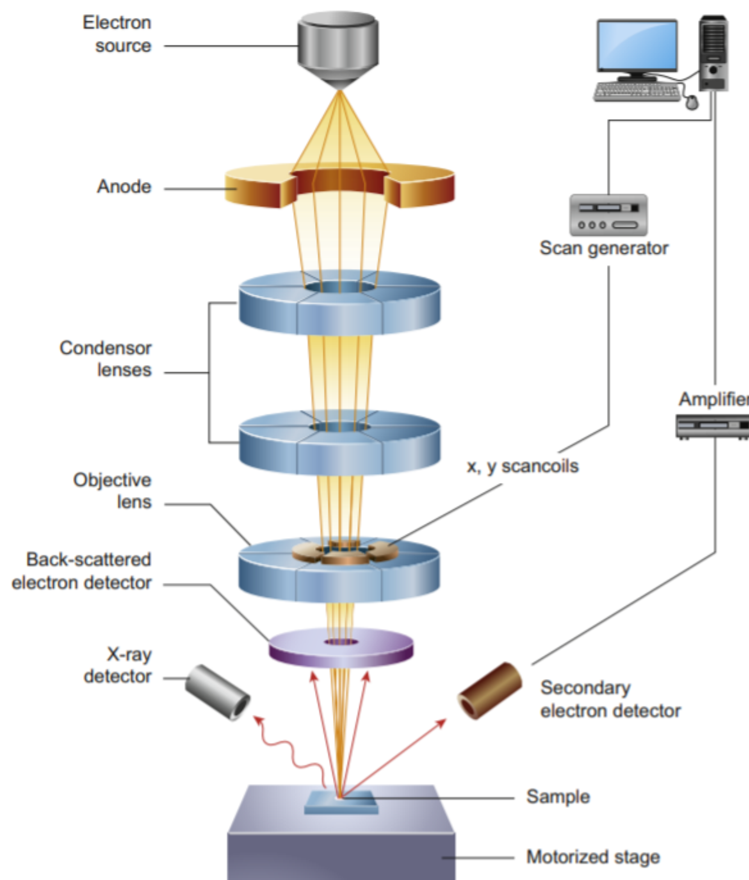

Figure 2.5: Schematic illustration of a SEM microscope [17].

SEM stands for scanning electron microscopy. It is an electron microscope that scans the surface of a specimen providing a high-resolution imaging. The various signals that are produced during the scanning are used to obtain information about the surface topography and composition of the sample [18].

On the top of Fig.2.5 is depicted the electron source. A beam of electrons is generated by a thermionic gun which are accelerated by 1-30 kV. The beam goes through

a series of electromagnetic lenses in order to control and focus the electron beam precisely on the specimen. In the final lens, a pair of scanning coils, that create two magnetic fields perpendicular to each other, is used to deflect the beam on x-y plane making feasible the scanning on the surface of the sample. The sample is placed in a vacuum chamber which is essential for the operation of SEM. The vacuum is needed to avoid the interference of the air's molecules with the electron beam that would result in the distortion of the image. The electron beam traces over the surface and a selection of detectors collects the emitted signals. The collected electrons of different levels of brightness, as the scanning occurs provide information about the scanned surface, which is recorded by a computer[19].

2.4 Photoluminescence

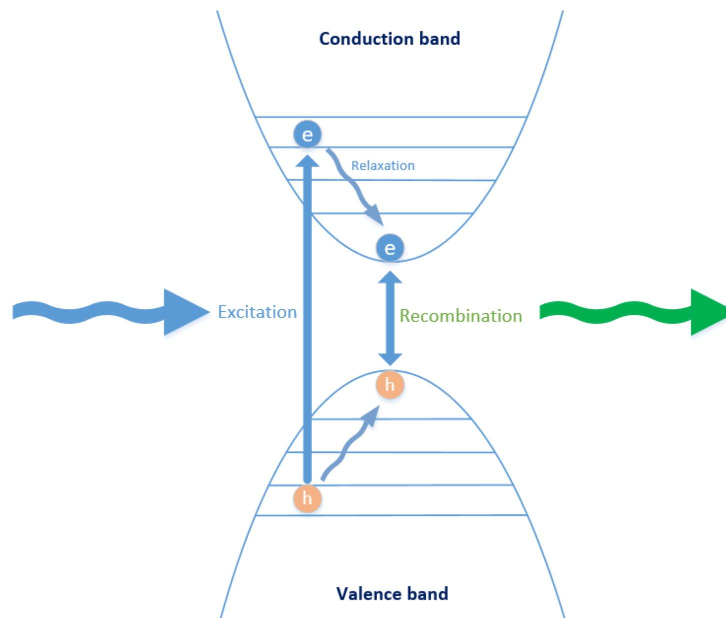

Figure 2.6: A schematic representation of photoluminescence mechanism.

Photoluminescence (PL) is the light emitted by a semiconductor after the absorption of electromagnetic radiation in form of photons. In a PL experiment, the semiconductor must be excited with photons that have greater energy than the semiconductor's band gap. Once the photons are absorbed, electrons and holes are formed in the conduction and valence band respectively, which then rapidly relax down to the band extrema.

Finally the electrons and holes recombine, emitting photons which are characteristic of the system at hand. [20].

In Fig.2.7, the main parts of our PL set up are shown. A He-Cd 325nm CW laser source with an energy $hv > E_g$ was used to excite our sample. The beam follows a path through mirrors, filtered by an iris and then focused by a lens on the sample. The sample, in turn, is placed inside a cryostat, which can cool the sample using a closed-cycle liquid Helium cooler, in the temperature range 14-300K. After the excitation, the signal from the sample is collected by a large diameter collection lens which is then focused to a spectrometer, connected to a CCD camera.

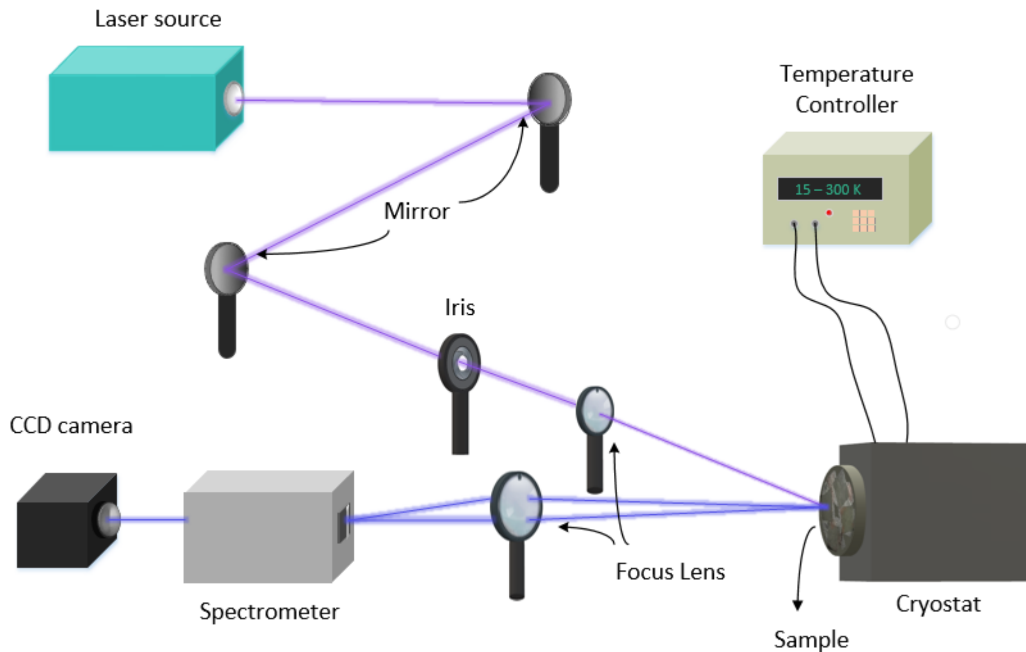

Figure 2.7: Schematic depicts the PL set up.

2.5 Atomic Force Microscopy

Atomic Force Microscopy (AFM) was originally developed by IBM scientists in the early 1980's and it is a form of scanning probe microscopy (SPM) with high resolution on the order of nanometers in the x-y plane and sub-nanometers in the z-direction [21]. An

AFM system can be used for surface imaging and force measurement. This information can be obtained by either "feeling" or "touching" the surface of the sample. The reaction of the probe to the forces between the tip and the surface of the sample are used to generate a 3D image of the sample's surface.

The AFM uses a cantilever with a sharp tip to scan the surface of the sample. As the tip approaches the surface, attractive forces cause the cantilever to deflect towards the surface. When the cantilever is brought very close to the surface so the tip "touches" the sample, repulsive forces cause the cantilever to deflect away from it. To detect the cantilever's deflections a laser beam is used. The small changes in the position of the reflected beam are detected by a position sensitive photo-diode. Then by using a feedback loop AFM is able to generate an accurate surface map [22]. In Fig.2.8, an AFM system is shown.

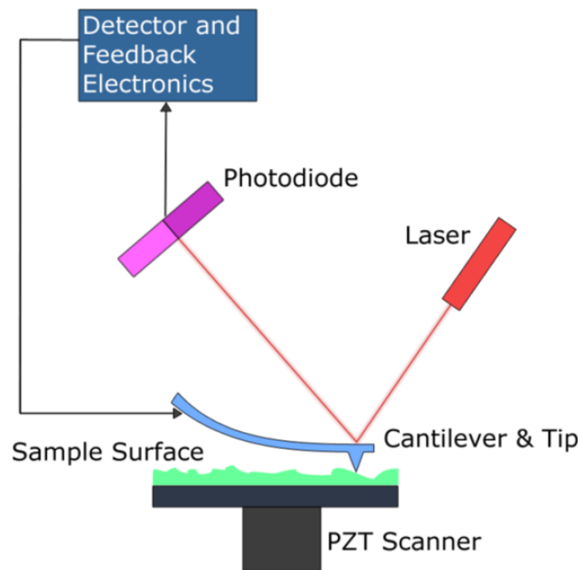

Figure 2.8: A schematic representation of an AFM system.

2.6 Transfer

For the purposes of membrane transfer process we used Polydimethylsiloxane (PDMS). PDMS is a polymer organosilicon compound and is particularly known for its rheological

(or flow) properties [23]. The PDMS empirical formula is (C2H6OSi)n, where n is the number of monomers repetitions. PDMS can be liquid or semi-solid depending on the size of monomers chain. Liquid PDMS can be also mixed with a cross-linking agent and be heated up in order to obtain solid PDMS. [24] In addition, solid PDMS is transparent and flexible and due to its properties can be used as medium for transfer not only of bulk semiconductors but also of two-dimensional materials [25]. Fig.2.9 depicts our transfer process by using PDMS. Firstly, PDMS is placed in contact with the surface of the sample. By pushing slightly the top surface of PDMS, the free-standing GaN membrane is strongly attached to it . Then, by removing the PDMS abruptly, we lift up the GaN membrane which is now adhered to the bottom of PDMS. The next step is to place the PDMS/GaN on the surface of a SiO_2/Si substrate. Finally, we remove slowly the PDMS in order to free the GaN membrane on the template.

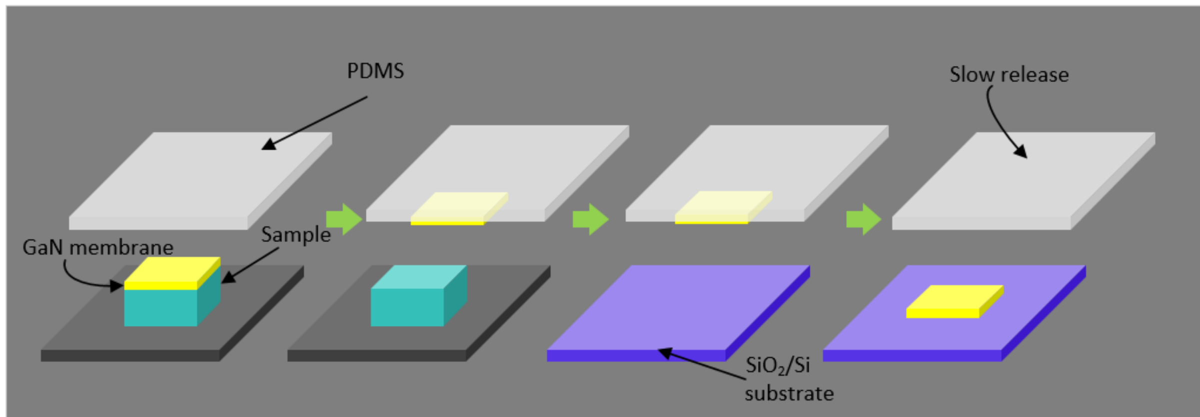

Figure 2.9: A schematic representation of transfer process.

Chapter 3

Experiments on a First Set of Samples

3.1 Introduction

In this chapter, we are going to analyze the experiments that have been carried out on a first set of samples. Firstly, we are going to describe the fabrication of the as grown samples and their characterization. In addition to this, we are going to discuss their modification to mesas as well as the PEC etching technique in order to enable the free-standing GaN membranes. Finally, we are going to optically characterize our membranes and conclude on our results.

3.2 Structure

The first series consists of three samples with code names E3933,E3934 and E3935. The design of these samples is the outcome of previous studies which have also used PEC etching technique on similar structures with InGaN as a sacrificial layer.

The structures consist of a c-axis 4 μm n-type GaN (non-intentionally doped) which is grown on a sapphire substrate. The next three layers consist of a heterostructure AlGaN/InGaN/GaN, which is grown by molecular beam epitaxy (MBE).The AlGaN layer whose aluminum content is ~ 7 % has a thickness of 500 nm. The idea of using this layer is

to absorb the incident light and prevent it from exciting the GaN at the base. This way the emission of the thin GaN on the surface would be distinguished in the Photoluminescence spectrum. With regard to the next layer, the thickness of InGaN is 5 nm with a nominal indium content of ~ 14 %, which was chosen in order to be suitable to the PEC etching conditions. On the top of these layers, there is the GaN membrane whose thickness differs in the three samples. The samples E3933, E3934 and E3935 have GaN thickness of 30 nm, 5 nm and 10 nm, respectively. A schematic illustration of the samples is shown in figure 3.1.

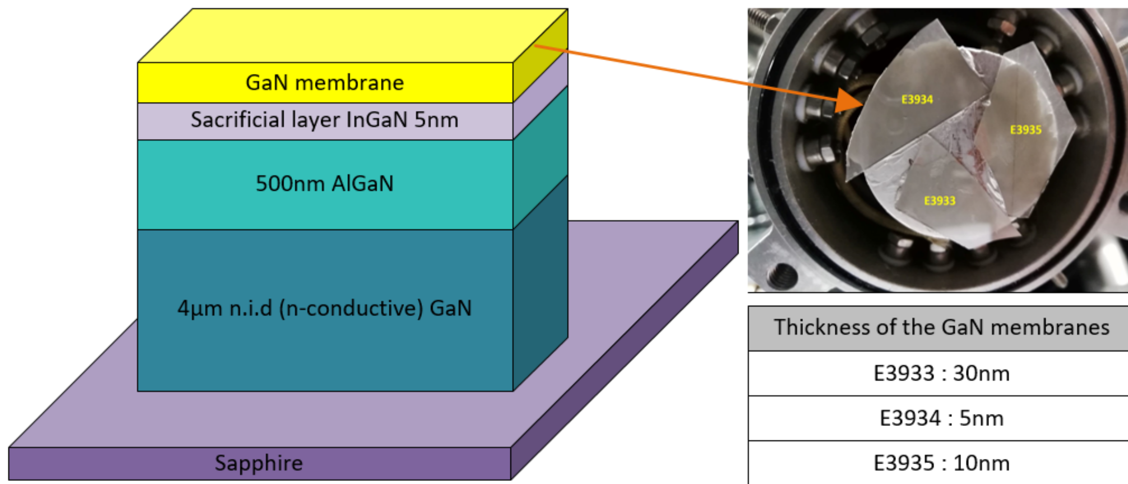

Figure 3.1: Schematic depicts the design of samples E3933, E3934 and E3935.

3.3 Characterization of as-grown samples

In this section, measurements on the as-grown samples have been done in order to characterize them. Firstly, photoluminescence and reflectance measurements were performed to examine any deviations from the theoretically designed structures. Secondly, Atomic Force Microscopy measurements have taken place to check the roughness of their surface. Finally, XRD reciprocal mapping was performed in order to extract information about the strain state and composition of the AlGaN layer.

3.3.1 Photoluminescence and Reflectance

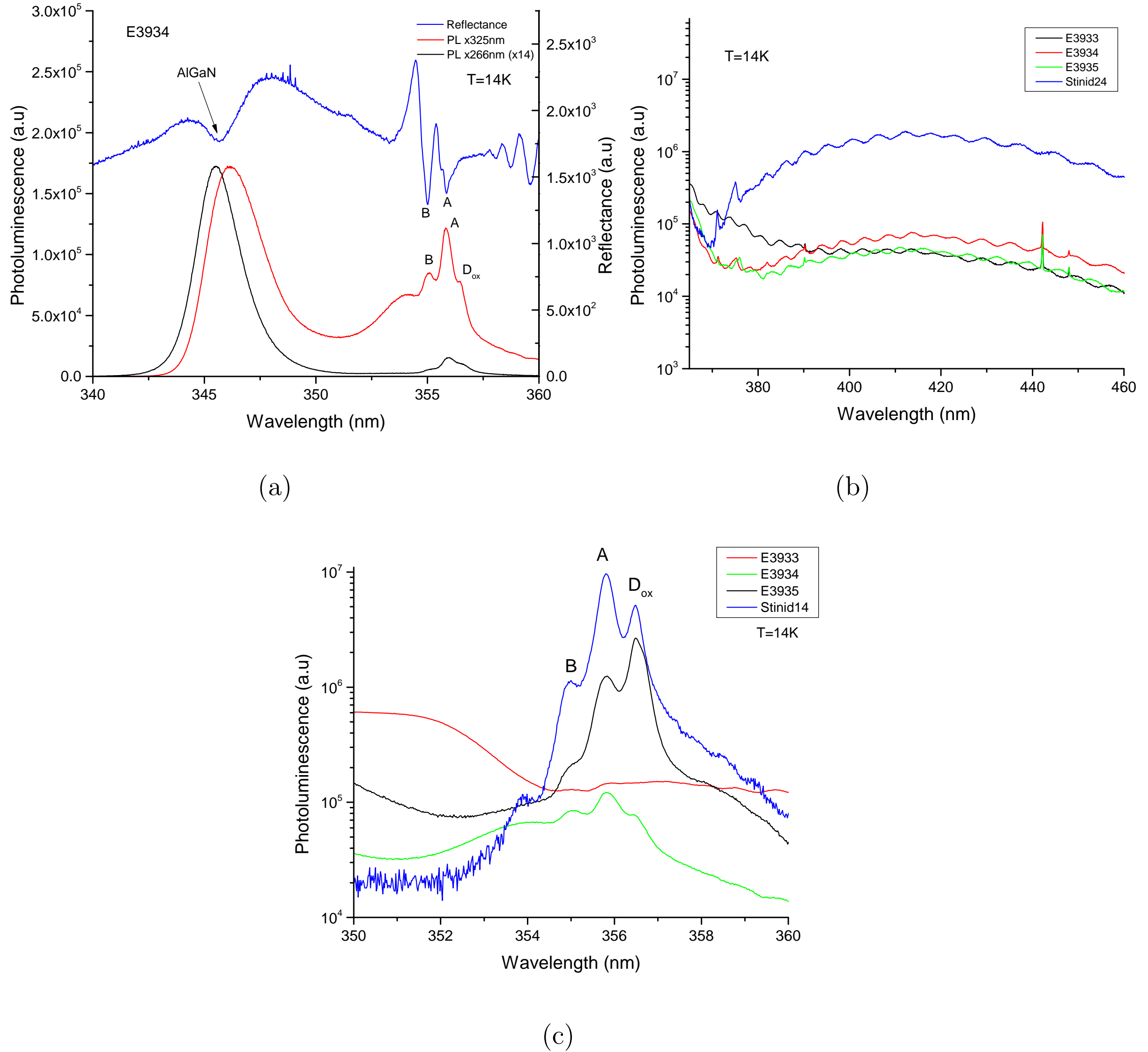

Figure 3.2: PL measurements in the spectral range of (a) AlGaN, (b) InGaN and (c) GaN emission.

In Fig.3.2a, we plot a characteristic PL spectrum of one of the samples (E3934) and compare it with the respective reflectivity (RFL) spectrum. In the RFL spectrum, we observe a strong exciton feature at $\sim$ $345nm$ which corresponds to the thick AlGaN layer, accompanied by an intense PL emission peak at about the same wavelength. From

the wavelength position of the AlGaN, we deduce the Al-composition, x, based on the following relation in eV:

$$E_{g,AlGaN}(14K) = E_{g,GaN}(14K)(1-x) + E_{g,AlN}(14K)x - bx(1-x) - 240 \cdot 10^{-3}x \quad (3.1)$$

where the last term is due to the tensile strain in this layer, as confirmed by the XRD reciprocal space mapping discussed below. The estimated x_{Al} is $\sim 7\%$ in good agreement with XRD. At lower energies, we observe in RFL the A and B excitonic features of GaN which correlate well with corresponding peaks in PL. These peaks seem to co-exist with deep-level emission from the AlGaN layer, which makes it difficult to observe any weaker features possibly related with the top GaN layer.

In Fig.3.2b, we compare the PL emission of the three samples in the 380-460 nm range, where the InGaN's PL emission is expected. We observe a broadband emission which cannot be attributed to the InGaN sacrificial layer, as it is also present in the PL emission of the underneath GaN template. Thus, no information can be gathered from PL about the InGaN composition in this set of samples.

Finally, in Fig.3.2c, we zoom-in at the PL emission of all samples at the GaN band-edge and compare with the reference GaN-template. We observe large intensity and spectral variations from one sample to the other, which at this stage we cannot exclude the possibility that they are due to a varying optical quality of the GaN template in the different samples.

Moreover, as pointed above, it is not possible to observe any weak PL peak, associated with the top-GaN layers, due to the relatively strong deep-level emission from the AlGaN layer and bandedge emission of the GaN template in the same spectral region.

3.3.2 Atomic Force Microscopy

AFM measurements were performed on samples E3933 and E3935 in order to get information about the roughness of our samples. Our results are shown in Fig.3.3. The GaN surfaces exhibit root-mean square (R_{ms})) roughness values around $\sim 1nm$, which is

relatively high compared to other GaN films grown by MBE. However, this is a typical value for AlGaN/GaN heterostructures, as in our case [26]. Moreover, there are bright spots on both samples, which are due to dislocations (pyramid-shaped), whose density is around $10^8 cm^{-2}$. Finally, there are tiny bright spots on the samples which are most likely due to some kind of contamination during handling of the samples.

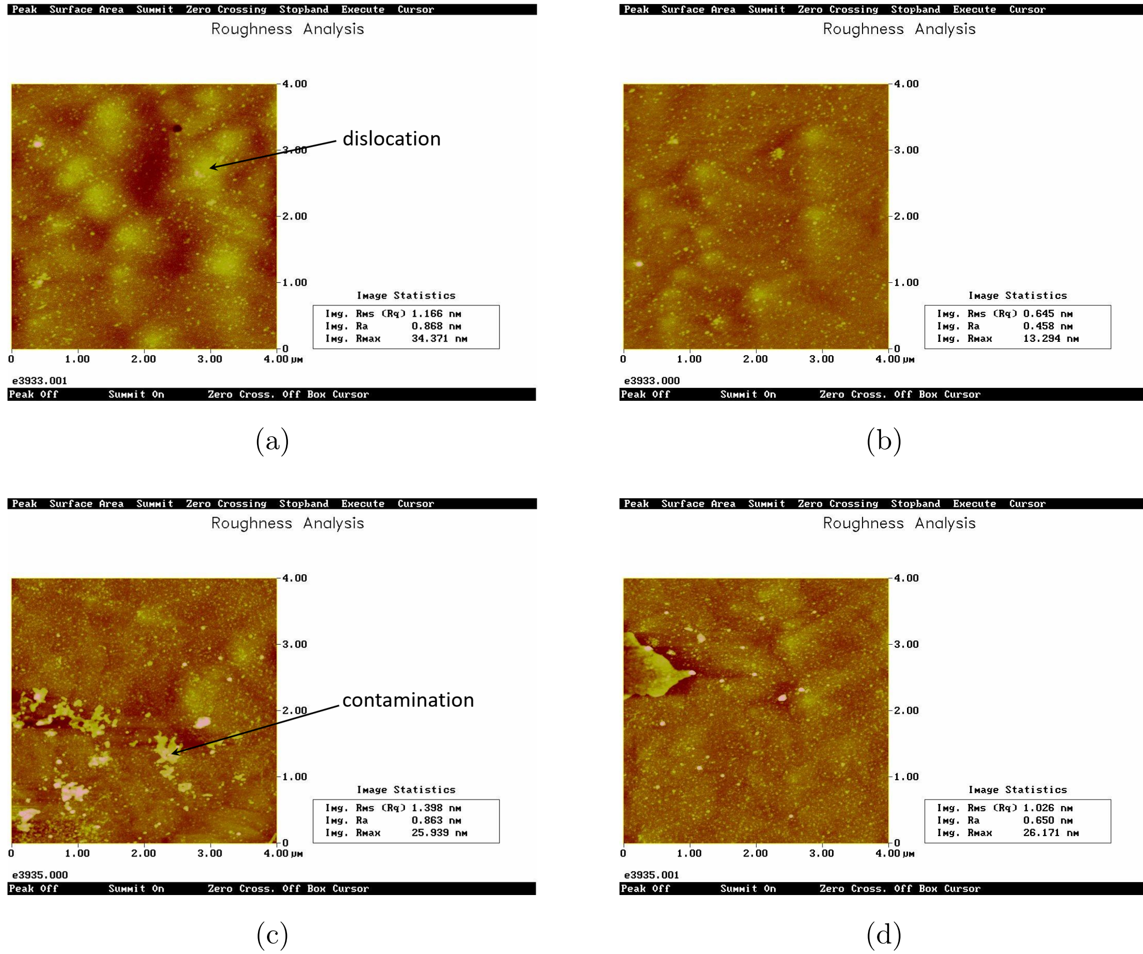

Figure 3.3: AFM measurements on samples (a)-(b) E3933 and (c)-(d) E3935.

3.3.3 XRD measurements

XRD Reciprocal Space Mapping measurements were performed on sample E3933 in asymmetric reflection (104) in order to examine the strain of the half-micron thick AlGaN layer. Fig.3.4 shows that both GaN and AlGaN peaks correspond to the same in-plane

lattice meaning that the AlGaN is fully strained on GaN. In addition, by performing a $\theta - 2\theta$ scan, we measured the lattice constant c for AlGaN by using the Bragg's law (2.3) . In case of hexagonal structures, the interplanar distances are

$$d_{hkl} = \frac{a}{\sqrt{(h^2 + k^2 + hk) + \frac{a^2 l^2}{c^2}}}. \tag{3.2}$$

Thus, at the asymmetric reflection plane (002), the lattice constant $c = 2d_{hkl}$. By taking the X-ray wavelength $\lambda = 1.540\,56$ Å and $\theta = \theta_i + \Delta\omega$ where the critical angle for GaN is $\theta_i = 17.2703°$ and $\Delta\omega$ the peak difference between GaN and AlGaN, the calculated parameter is $c_{meas} = 5.16863$Å (Fig.3.5). Taking into consideration that AlGaN layer has the same in-plane lattice constant with GaN ($a_{meas} = a_{GaN}$) and by using the following formulas, we estimated that the aluminum content is $\sim 6\%$.

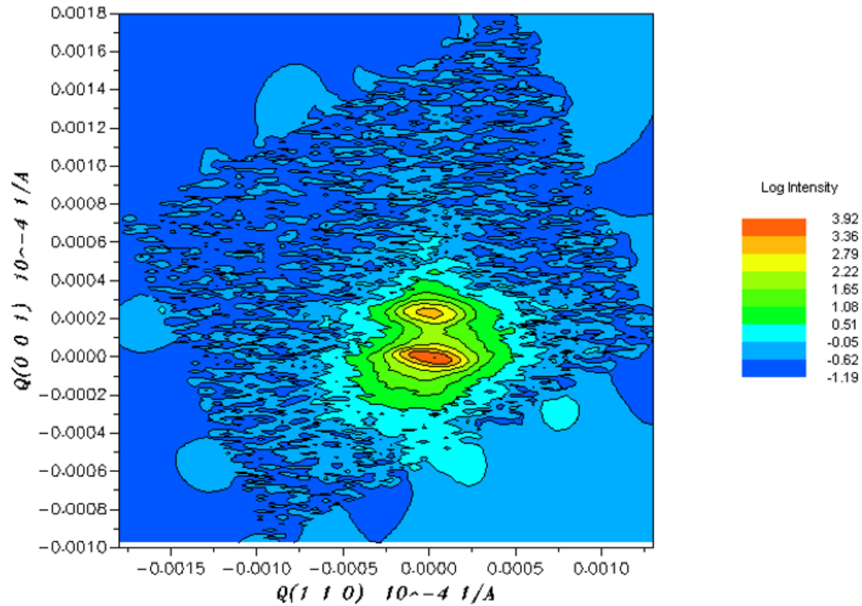

Figure 3.4: XRD reciprocal space mapping of E3933 showing the strain of AlGaN layer on GaN .

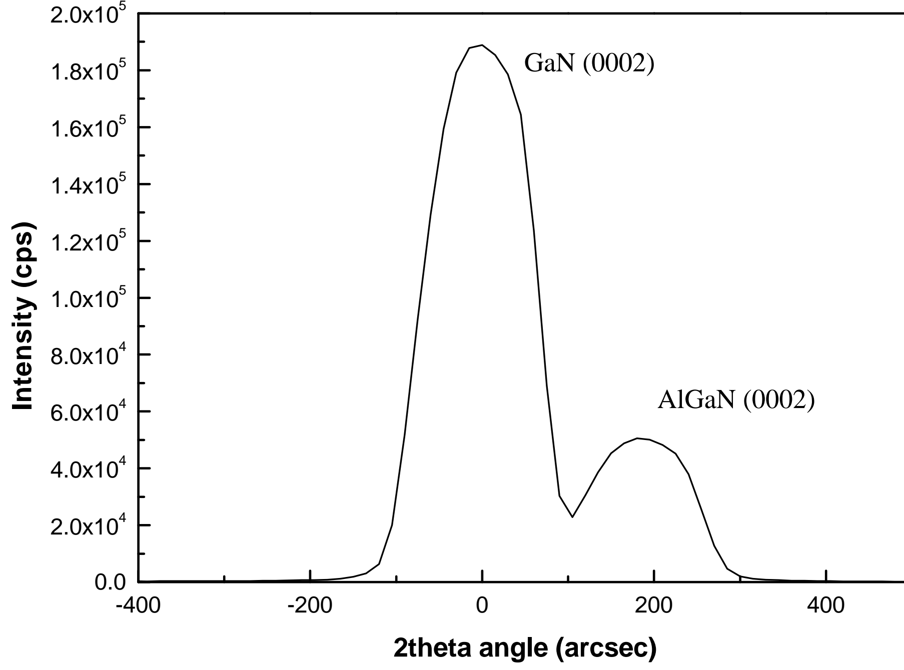

Figure 3.5: XRD theta-2theta scan of sample E3933

$$\frac{\Delta c_o}{c_o} = -2\frac{c_{13}}{c_{33}}\frac{\Delta a_o}{a_o} \tag{3.3}$$

where

$$\begin{cases} \Delta c_o = c_{meas} - c_o & (3.4a) \\ \Delta a_o = a_{meas} - a_o & (3.4b) \end{cases}$$

where $a_o(x)$, $c_o(x)$ are the relaxed values of $Al_xGa_{1-x}N$.

$$\frac{\Delta c_o}{c_0} = \frac{c_{meas} - [c_{GaN}(1-x) + xc_{AlN}]}{c_{GaN}(1-x) + xc_{AlN}} \tag{3.5}$$

$$\frac{\Delta a_o}{a_0} = \frac{a_{meas} - [a_{GaN}(1-x) + xa_{AlN}]}{a_{GaN}(1-x) + xa_{AlN}} \tag{3.6}$$

$$\frac{c_{13}(x)}{c_{33}(x)} = \frac{c_{13,GaN}(1-x) + xc_{13,AlN}}{c_{33,GaN}(1-x) + xc_{33,AlN}} \tag{3.7}$$

3.4 Design of MESAs

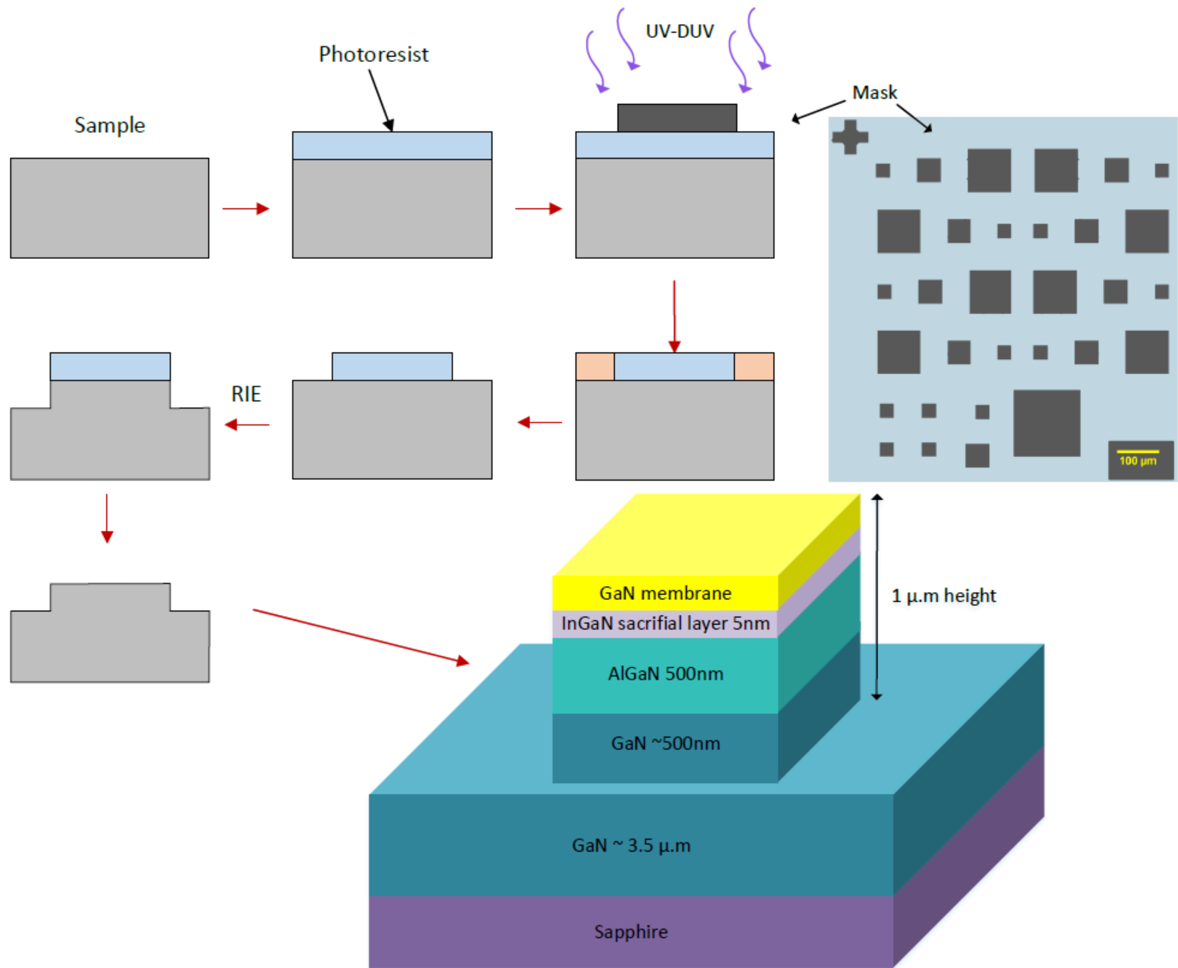

Figure 3.6: Schematic depicts the processing for the fabrication of $1\mu.m$-high of squared mesas.

After the characterization of the as-grown samples photolithography process and Reactive Ion Etching (RIE) took place, in order to create geometrical shapes (mesas) on the surface of the samples. This procedure is essential for PEC etching technique, as

it exposes laterally the InGaN sacrificial layer. The processing is described in the next paragraph.

Image Reversal resist $Z5214$ is spin-coated at 4000rpm in order to obtain homogeneous thickness on the surface of the sample. Then the sample is placed on a hot plate at 110°C for 20 sec to harden the resist. A metal mask with square mesas with various dimensions ranging from $45 \times 45\mu m^2$ to $155 \times 155\mu m^2$ is aligned on the sample followed by UV-DUV irradiation. Then the radiated photoresist is removed with $AZ400$ photoresist removal, diluted in DI water at 1:4 ratio to expose the desired areas of the surface. Reactive Ion Etching (RIE) technique is used to etch these areas and form the MESAS. Finally, the samples are rinsed in acetone followed by DI water in order to remove any photoresist residues and a profilometer is used to measure the etching rate, which was 15nm/min. Fig.3.6 shows the process flow by photolithography and RIE, as well as the metal mask that is used in order to modify the original samples into patterned $1\mu m$-high squared mesas.

3.5 Photoelectrochemical etching procedure

The PEC etching technique was initially implemented on a reference sample, E3805C, having a similar structure, where the sacrificial layer of InGaN is 20nm thick and the GaN-based membrane on the top is 200nm, in order to control the PEC set-up and the conditions of the process. By applying several sets of voltage, etching time, power and concentration of KOH solution, in accordance with previous work based on the optimization of PEC in similar structures for the fabrication of microcavities, we obtained the desired result, as shown in fig.3.7. In fig.3.7a is illustrated an optical microscope image where the membranes following successful etching are sitting on their mesas taking a light yellow colour arising from the reflection of the incident light, while the mesas in the surrounding area do not change colour as they remain unetched. This is more evident in the SEM image of fig.3.7b, where the GaN membrane is clearly lifted up. The PEC conditions that we applied here were: V=4Volts, P≈5.00mW, $C = 4 \cdot 10^{-4} M$, t=2,400sec.

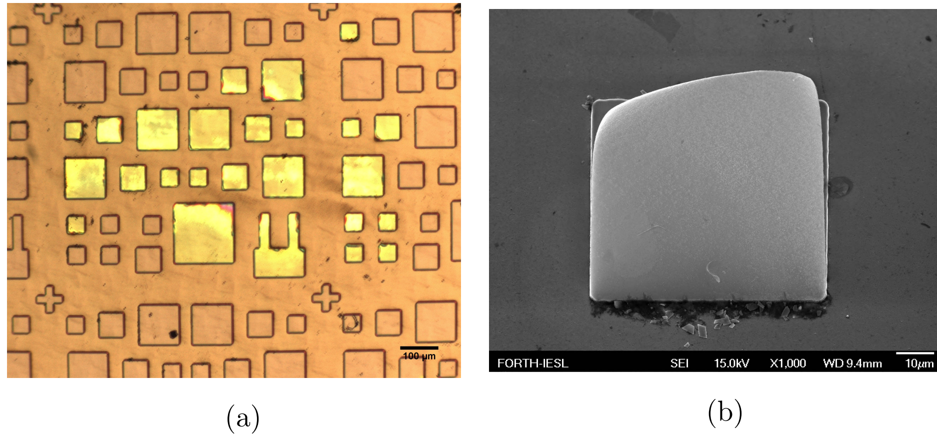

(a) (b)

Figure 3.7: PEC: V=4Volts, P≈5.00mW, $C = 4 \cdot 10^{-4}M$, t=2.400sec (a) An optical microscope image and (b) a SEM image of E3805C after etching.

Based on the results on sample E3805C, we applied the exact same conditions on the set of samples E3933-35, starting with E3933 where the GaN layer on the top of the structure is 30nm-thick. The results were not as expected as the surface of the GaN top layer was fully damaged after PEC (Fig.3.8). In the optical image, fig.3.8a, aside from a light greyish shadow on the PEC spot, the surface of the mesas shows no particular colour contrast with respect to their surroundings, at least in comparison with the reference sample (fig.3.7). Additionally, in the SEM images (fig.3.8b,3.8c), we can clearly confirm the damaged GaN membrane.

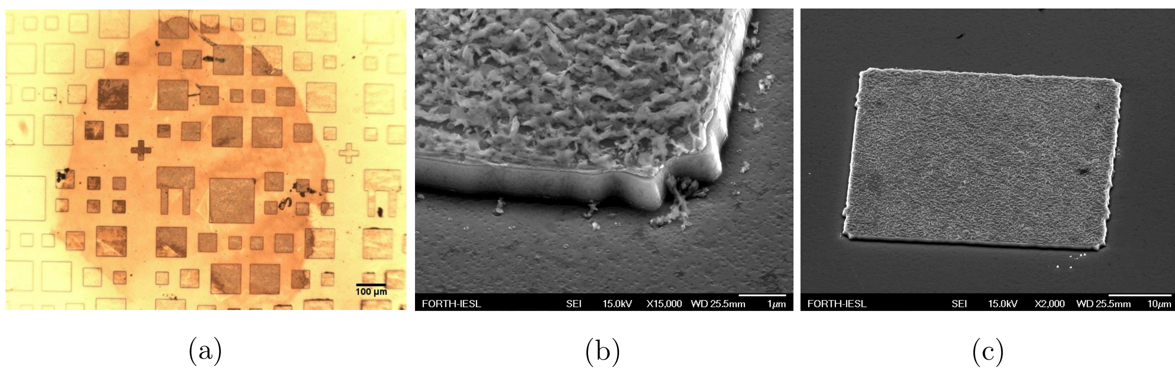

(a) (b) (c)

Figure 3.8: PEC: V=4Volts, P≈5.00mW, $C = 4 \cdot 10^{-4}M$, t=2,400sec (a) An optical microscope image and (b),(c) SEM images of E3933 after etching.

By keeping constant the voltage, laser power and concentration of KOH solution

we decreased the time down to 1500sec. In the optical image of fig.3.9a, there is no evidence of improvement whereas in the SEM images, there is a somewhat less damaged surface (fig.3.9b-3.9e), but without any clear indication of a lifted membrane.

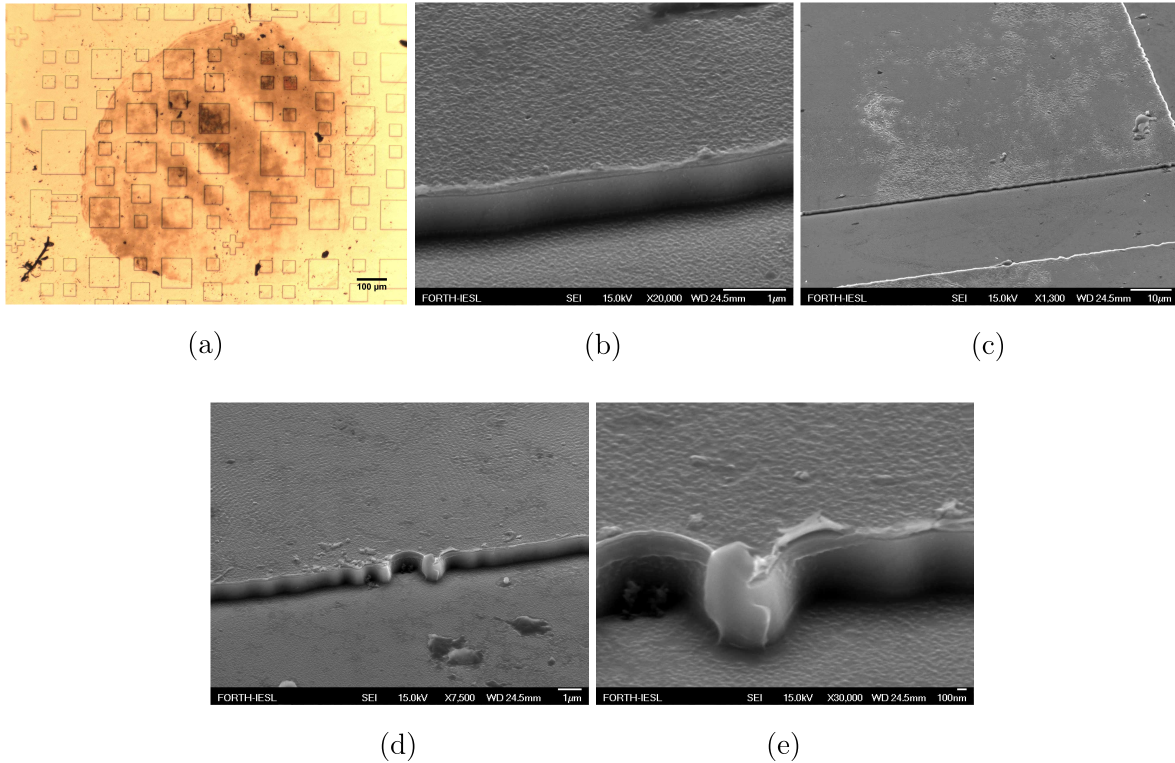

Figure 3.9: PEC: V=4Volts, P≈5.00mW, $C = 4 \cdot 10^{-4} M$, t=1,500sec (a) An optical microscope image and (b)-(e) SEM images of E3933 after etching.

In order to decrease further the damage of the membranes' surface, we performed another run with the same conditions but even less time, 650sec. The results are shown in Fig.3.10. In the optical microscope image, we observe the same greyish coloration of the PEC spot, a little fainter compared to the larger etching times (c.f. 3.9, 3.8). In the SEM images, however, one observes on the mesas' surface the appearance of distinct holes, suggesting that the etching did not go only laterally but that the electrolyte somehow penetrated and reacted with InGaN layer from the top surface of the mesas.

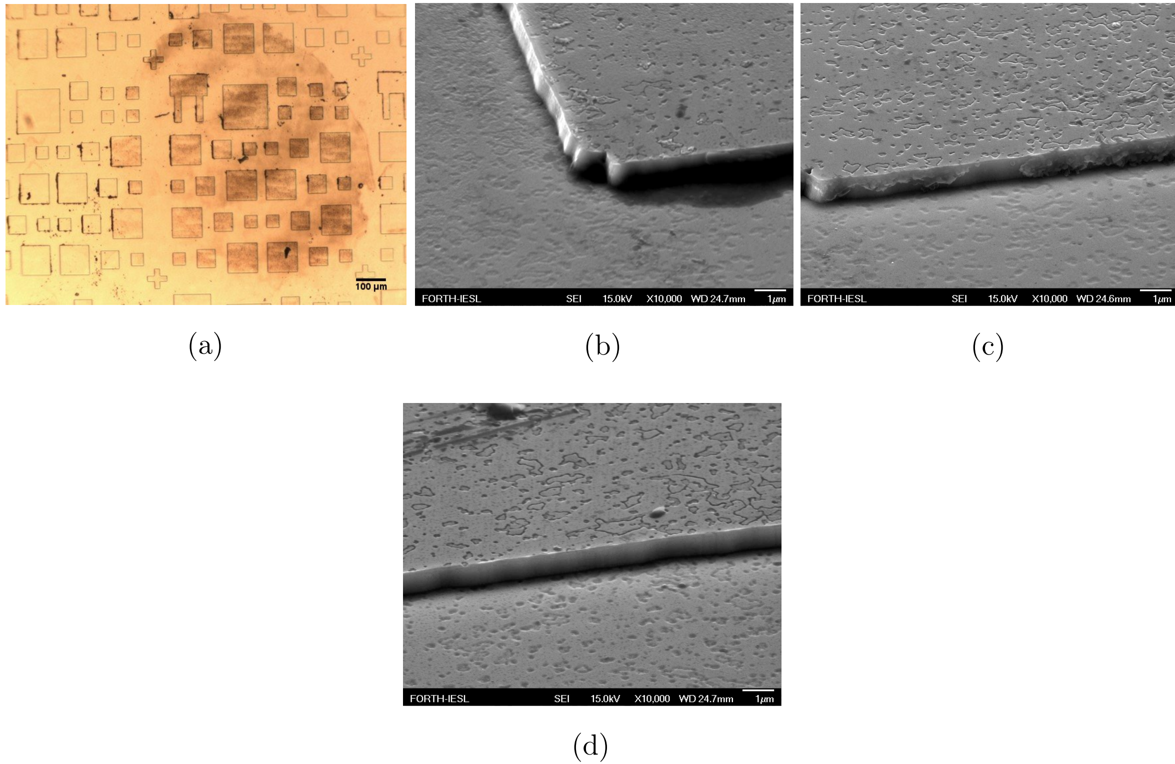

(a) (b) (c)

(d)

Figure 3.10: PEC: V=4Volts, P≈5.00mW, $C = 4 \cdot 10^{-4}M$, t=650sec (a) An optical microscope image and (b)-(d) SEM images of E3933 after etching.

In order to confirm the previous result, we applied the same conditions on sample E3935, which has a 10nm top-layer of GaN. The results were not similar with those of sample E3933 (fig.3.10). As shown in fig.3.12, in both optical and SEM images, several mesas showed in part of their area "vertical" etching whereas in the remainder they seemed intact or their surface appeared uniform. No sign of "clean" lateral etching was found either in this sample.

As a next step, in order to improve the etching results, we decreased the concentration of OH^- by a decade to $C = 4 \cdot 10^{-5}M$. The idea was that as the sacrificial layer of InGaN is 5nm thick in comparison with the reference sample E3805C where the InGaN membrane was 20nm, perhaps the rate of photoelectrochemical reaction should be decreased in order to obtain smooth lateral etching of the GaN membranes. Looking at the SEM images (fig.3.11b-3.11e), the results appeared similar with the previous run (fig.3.12) in the sense that there are still holes on the GaN surface. However, overall, the

top surface appears more uniform which could indicate that the etching of InGaN was also uniform.

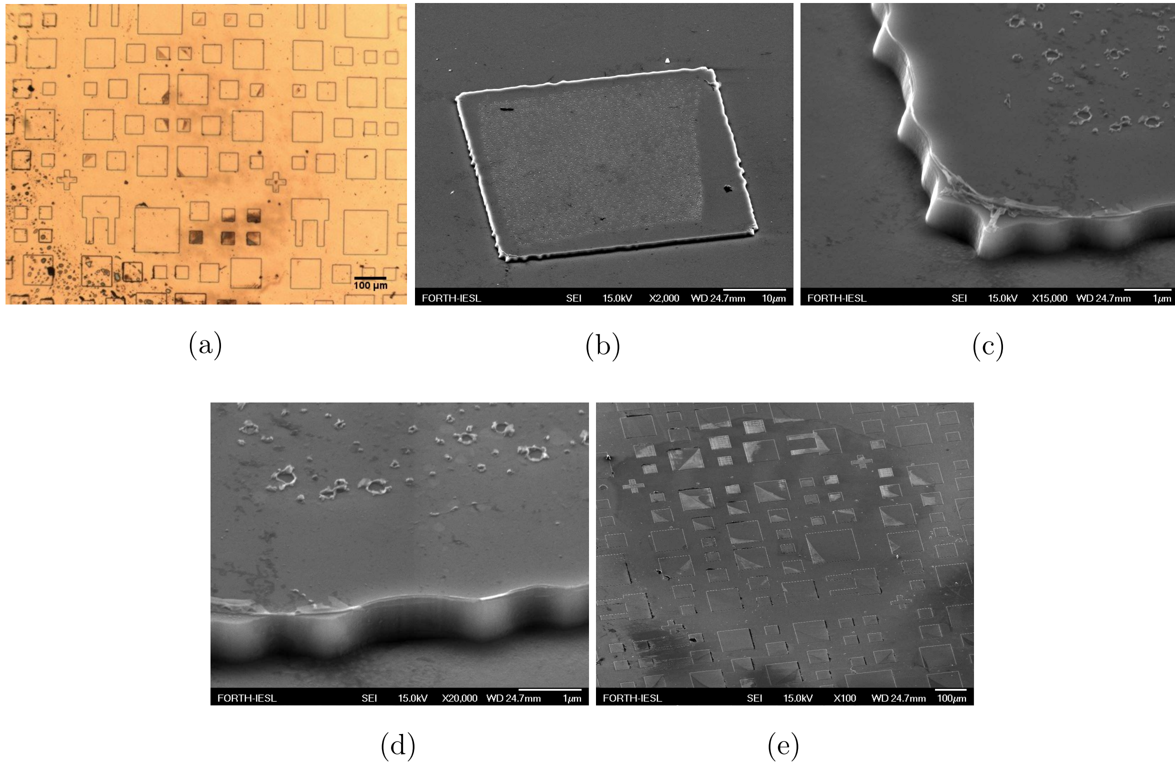

(a) (b) (c)

(d) (e)

Figure 3.11: PEC: V=4Volts, P≈5.00mW, $C = 4 \cdot 10^{-5} M$, t=600sec (a) An optical microscope image and (b)-(e) SEM images of E3935 after etching.

Finally, we applied the same conditions on the same sample, by increasing the time up to 940sec. As shown in the optical image fig.3.13a, most of the mesas have a dark grey colour and some of them a slight yellow. In the SEM images (fig.3.13b-3.13d), it seems to be clear that the mesas are overetched and that "vertical" inhomogeneous etching occurred, leaving the surface of the GaN membranes partially damaged with many holes.

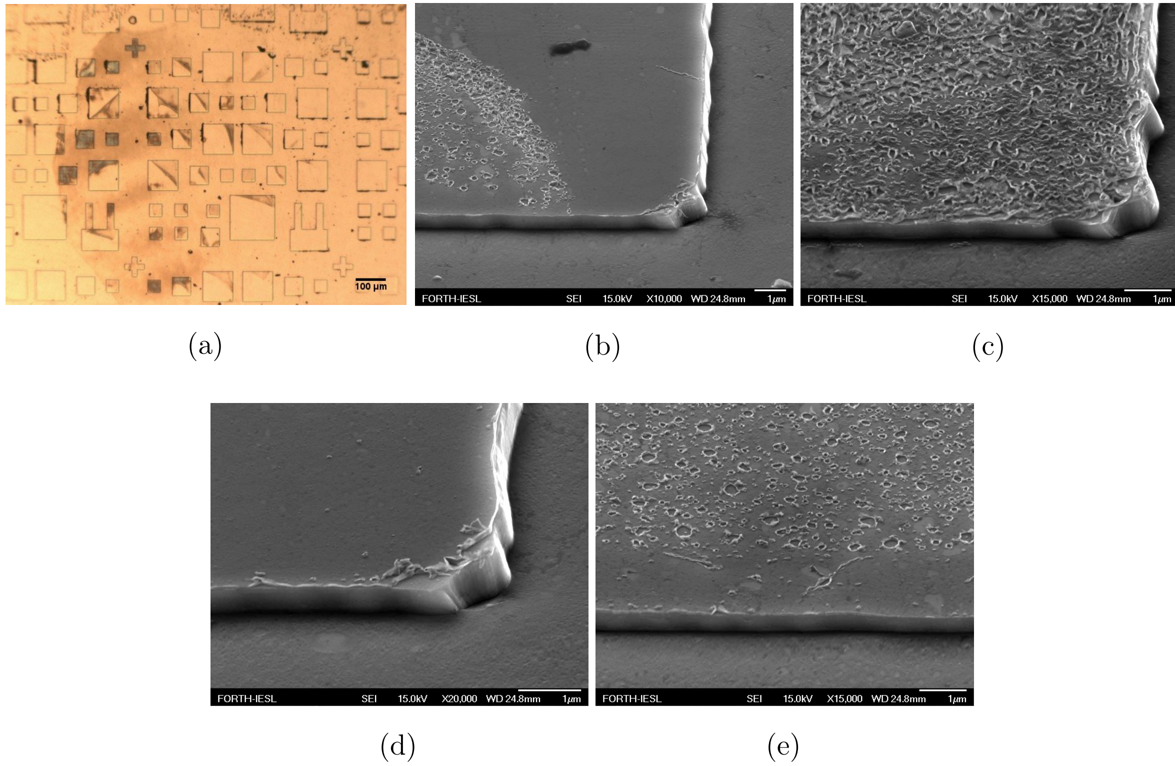

Figure 3.12: PEC: V=4Volts, P≈5.00mW, $C = 4 \cdot 10^{-4} M$, t=600sec (a) An optical microscope image and (b)-(e) SEM images of E3935 after etching.

Summarizing the above, by decreasing the etching time and concentration of KOH solution, we tried to optimize the PEC etching conditions in the first set of samples. The results were not satisfying as we didn't obtain any smooth membranes. What seemed characteristic in all these results was the "holes" on the surface of the GaN membranes in both samples we tried. The fact that the etching procedure was not just lateral but occurred also vertically could be attributed to pre-existing holes/defects on the surface of the as-grown samples, forming a pathway for the solution to react with the InGaN layer. Looking carefully at the SEM images of the as-grown samples, it is true that in sample E3933, there were in parts of the sample groove-like defects on the surface. But this was only in part of one of the three samples. Another possible explanation of the unsuccessful etching experiments can be based on the increased rms roughness in these samples, most likely due to presence of the thick AlGaN buffer layer. The increased roughness of AlGaN may have adversely affected the composition-profile of the InGaN layer, such that only islands of sufficient In-composition could participate to etching. Such

non-uniformity could explain the vertical etching and the fact that we failed to observe any clear indication of lateral etching such as a lifted-up membrane.

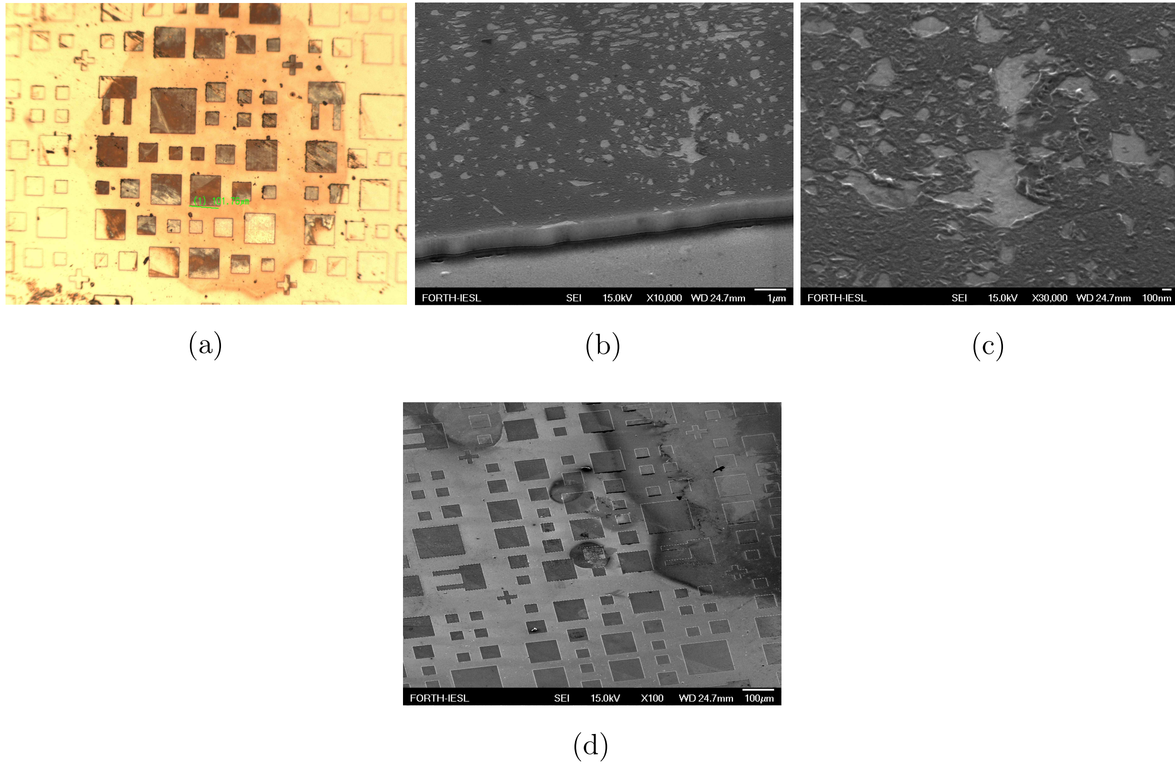

(a) (b) (c)

(d)

Figure 3.13: PEC: V=4Volts, P≈5.00mW, $C = 4 \cdot 10^{-5}M$, t=940sec (a) An optical microscope image and (b)-(d) SEM images of E3935 after etching.

In all the above discussion, we have tacitly assumed that the InGaN composition was close to nominal ($\sim$ 14%). Unfortunately, the 5nm-thickness of the sacrificial layer in this set of samples did not allow us to confirm this composition in an XRD $\theta - 2\theta$ scan. Moreover, the InGaN layer was not visible in the PL spectra either, due to strong deep-level emission from the GaN substrate in the spectral region of interest (380-460nm). However, based on later findings, in the second set of samples, discussed on chapter 4, we have good reason to believe that the In-content of the InGaN layer was smaller than 7.5% in the first set of samples as well. Such composition is really marginal in the sense that the 405nm laser is absorbed in the inhomogeneously broadened band-edge tail of InGaN. This would explain the inhomogeneous unsatisfying etching observed in the PEC experiments of this section.

3.6 Transfer

After the PEC etching procedure, we tried to transfer the inhomogeneously etched GaN membranes by using a PDMS stamp from the mesas to a $Si0_2/Si$ substrate in order to optically characterize them. However, as we previously mentioned, we did not manage to obtain any smooth GaN membranes with the PEC etching technique. As we shall see, only small fragments of GaN membranes were available for transfer. These small GaN pieces were strongly attached to PDMS leading to the unsuccessful transfer of them onto SiO_2/Si substrate.

In the images of Fig.3.14, we illustrated a spot from which we managed to extract some membranes on PDMS. The red frame around images denotes "before transfer" and the blue frame "after transfer". The first two optical images, fig.3.14a,3.14b, show the PEC spot before and after transfer on the sample E3935. Fig.3.14a presents a spot where some mesas have a dark grey colour and some of them a slight yellow (red circle). After transfer, there is a slight colour difference of mesas' surface which is more visible in the three mesas in the red circle (Fig.3.14b). The next two images show the transferred GaN membranes on PDMS, where in fig.3.14c the GaN is sandwiched between SiO_2/Si substrate and PDMS increasing their reflectivity contrast, where as in fig.3.14d the GaN membranes on PDMS are facing the air. In addition, we explain the colour change of the mesas in Fig.3.14a-3.14b as these areas were successfully transferred on PDMS. Moreover, SEM images 3.14e-3.14g provided more information about the surface of mesas before and after transfer. Fig.3.14e shows a SEM image of the etched area before transfer whereas in Fig.3.14f after transfer. Small pieces of mesas' surface were removed during transfer procedure, which is more evident in Fig.3.14g where there are small holes on the remaining GaN surface. The GaN membranes are multi-fractured having as a result to the unsuccessful transfer of them onto SiO_2/Si substrate.

After transfer, we tried to characterize the extracted GaN membranes on PDMS. Firstly, we tried to perform $\mu Raman$ measurements However, we did not manage to get any signal from GaN membranes, as the background signal from PDMS was extremely high in comparison with the weak signal of GaN fragments. Next step was their observation of them with SEM. The following SEM images show the GaN membranes on PDMS, for which some metallization was necessary to avoid charging effects during SEM

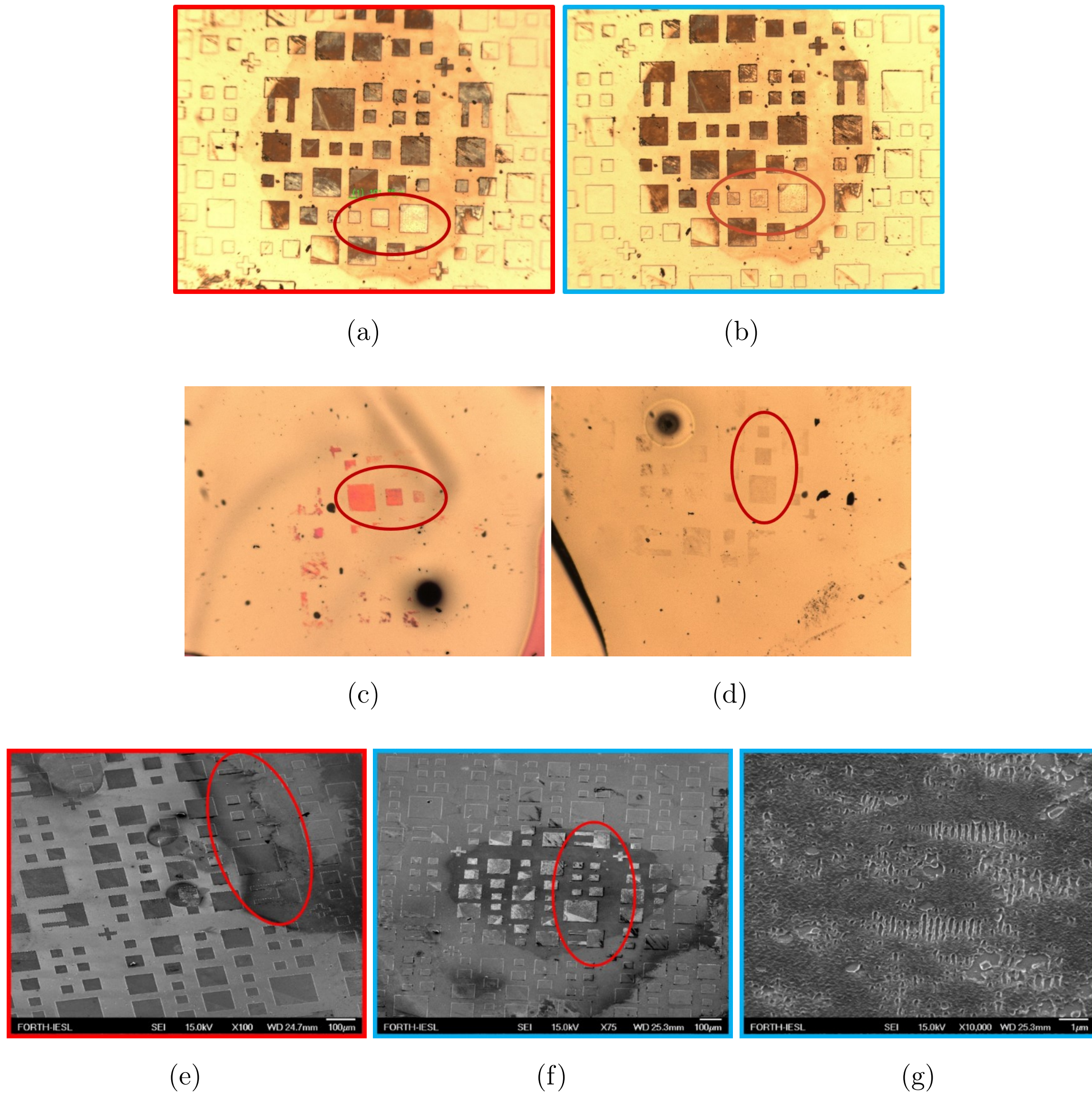

Figure 3.14: E3935: Optical images of (a) the PEC spot before transfer and (b) after transfer, (c) PDMS/GaN/SiO_2/Si substrate and (d) GaN/PDMS/SiO_2/Si substrate. SEM images of the same spot area (e) before and (f), (g) after transfer.

(Fig.3.15a-3.15e). It is clear that the surface of the membranes is multi-fractured into small pieces.

To summarize the above, we did not manage to transfer successfully the GaN membranes on the SiO_2/Si substrate. As GaN is fully damaged and PDMS has high flexibility, the membrane fragments are strongly attached to the PDMS. Moreover, based

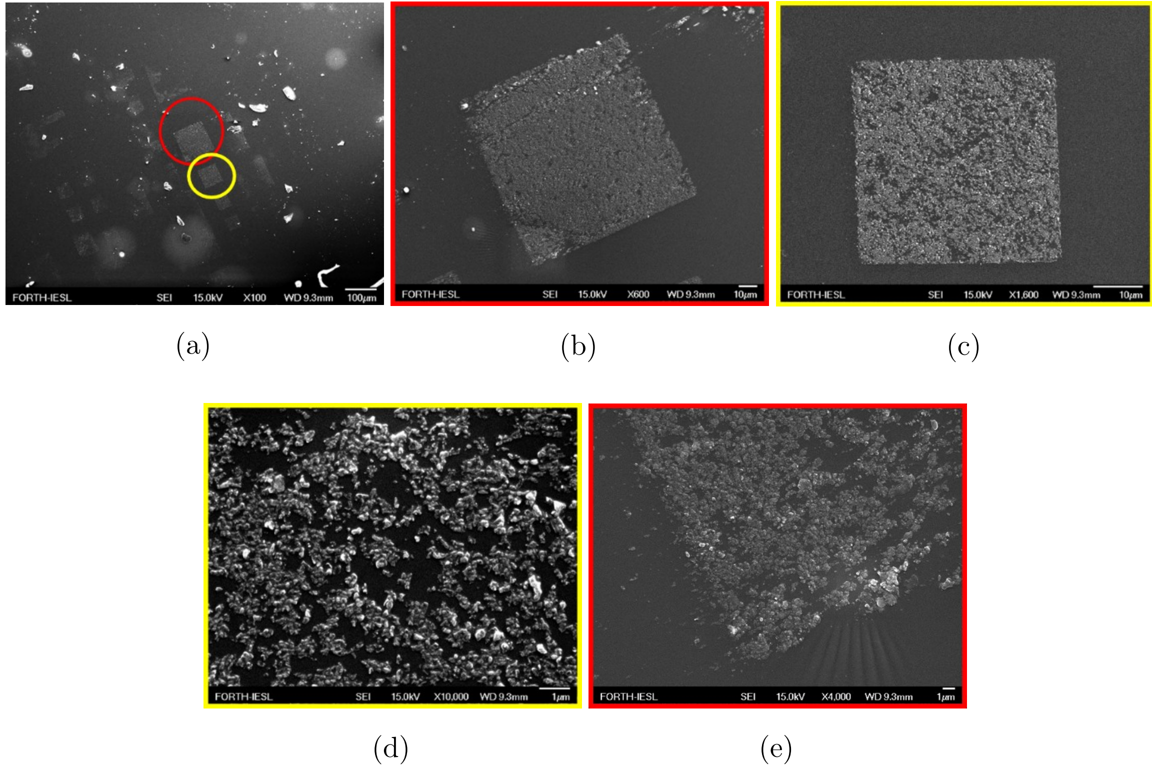

Figure 3.15: SEM images of GaN membrane fragments attached to PDMS.

on later findings, the indium consistency in the InGaN sacrificial layer played an important role for the fabrication of smooth GaN membranes. As a result of this, the transfer with PDMS of small GaN pieces was not feasible.

3.7 Conclusions

To sum up, the PEC etching technique for the fabrication of GaN membranes on the first set of samples E3933-35 did not turn out successful as we did not manage to obtain any smooth GaN membranes. At the time, we finished these experiments, we thought that the presence of AlGaN layer in our heterostructure, did not favour the PEC etching experiments, as the AlGaN layer increased the GaN membrane roughness as observed in AFM and possibly affected the homogeneity of In-composition in the InGaN layer, favouring inhomogeneous vertical etching versus standard lateral InGaN etching. Based on these considerations, we decided to ask for a second of samples, having the AlGaN

layer removed. A posteriori, having worked on the 2nd set of samples as well, we can say that it is quite likely that the In-composition of the first set of samples was much less than the nominal, accounting for the adverse etching results.

Chapter 4

Experiments on a Second Set of Samples

4.1 Introduction

In this chapter, we analyze the experimental measurements that have been carried out on a second set of samples without the AlGaN barriers following the conclusions of previous section. Firstly, we describe the structure and characterization of the as-grown samples. Next, we discuss the PEC results on these samples after the modification into mesas. Finally, we characterize some free-standing membranes and conclude.

4.2 Structure

The second series consists of three samples with code names E3981, E3982 and E3983. The design of these samples is based on the study of the previous set of samples, in order to improve the results of PEC etching technique for the fabrication of GaN membranes.

The structures consist of a c-axis 4 μm-thick n-type GaN template (non-intentionally doped) which is grown on a sapphire substrate. Our samples consist of a heterostructure

GaN/ InGaN/GaN, which is grown by molecular beam epitaxy (MBE). The thickness of InGaN is 20 nm in this series with a nominal indium content of ∼ 14 % to be suitable for the PEC etching conditions. On the top of these structures, there is the GaN membrane layer whose thickness differs in the three samples. The samples E3981, E3982 and E3983 have GaN thickness of 30 nm, 5 nm and 10 nm, respectively. A schematic illustration of the samples is shown in figure 3.1.

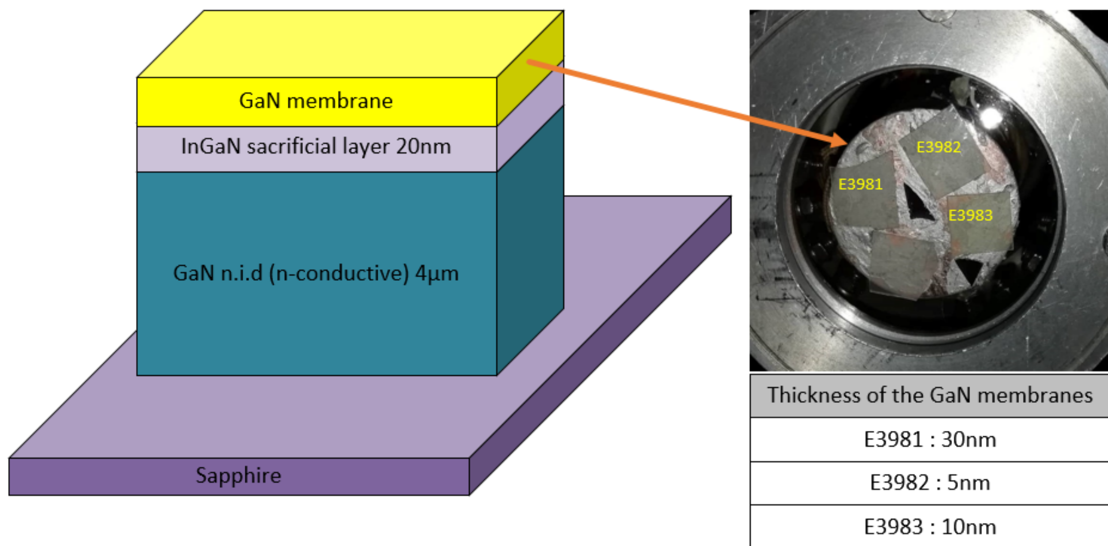

Figure 4.1: Schematic depicts the theoretical design of the samples E3981, E3982 and E3983.

4.3 Characterization of as grown samples

In this section, we describe the characterization of as-grown samples E3981-83. Firstly, photoluminescence measurements took place in order to assess the properties of the heterostructure GaN/InGaN/GaN. In addition, AFM measurements were performed to estimate the roughness of samples. Finally, XRD measurements took place in order to estimate the indium composition of InGaN sacrificial layer.

4.3.1 Photoluminescence

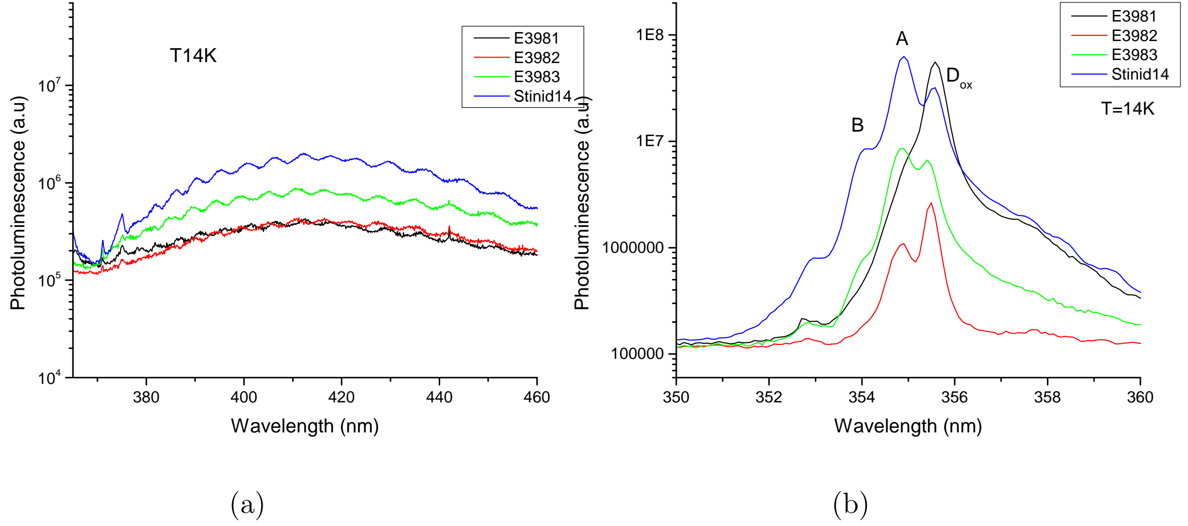

(a) (b)

Figure 4.2: PL measurements on the spectral range of (a) InGaN and (b) GaN emission.

Fig.4.2a shows the PL spectra in the spectral range of InGaN emission for the three samples. In addition, the PL spectrum of the underneath GaN template is also shown for comparison. Considering that the broadband emission is present for all three samples including the underneath template we conclude that we cannot extract information from PL about the InGaN composition in this set of samples.

Moreover, in Fig.4.2b, we zoom in at the GaN band edge emission of all samples at the GaN band-edge and compare with the reference GaN-template. In the semi-logarithmic PL spectra, we observe the Donor-band exciton line D_{ox}, as well as the free-exciton peaks A, B and C, with large variations in intensity from one sample to another. This variation cannot be reasonably attributed to the presence of the GaN membrane layer. At this stage, we cannot exclude the possibilities that the intensity variations are due to a varying optical quality of the GaN template in the different samples.

4.3.2 Atomic Force Microscopy

AFM measurements were performed on sample E3983 in order to examine the roughness of our samples. Fig.4.3 shows a root-mean square (R_{ms}) roughness values around $\sim 0.6nm$, which is significantly lower compared to previous results of the first set of samples ($\sim 1nm$ Fig.3.3). Moreover, the density of dislocations (pyramid-shaped bright spots) remains at $\sim 10^8 cm^{-2}$, which is normal as this corresponds to the substrate dislocation density which is the same in the two sets of samples. However, the tiny bright spots are much less than the previous set of samples.

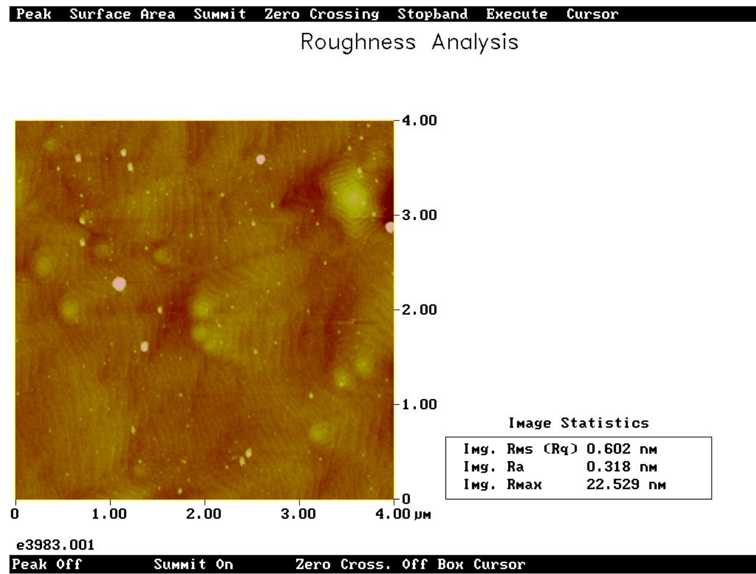

Figure 4.3: AFM measurements on E3983.

4.3.3 XRD measurements

XRD $\theta - 2\theta$ (Fig.4.4) scan was performed on sample E3982 in order to examine the nominal($\sim 14\%$) composition of indium in the InGaN sacrificial layer. Taking into account that InGaN layer is fully strained on GaN, we calculate the indium composition by using the following formulas 4.1-4.5. Considering that $a_{meas} = a_{GaN} = 3.18900$Å and that $c_{meas} = 5.24947$Å, we estimate the indium composition $\sim 7.4\%$, i.e. significantly lower than the nominal composition.

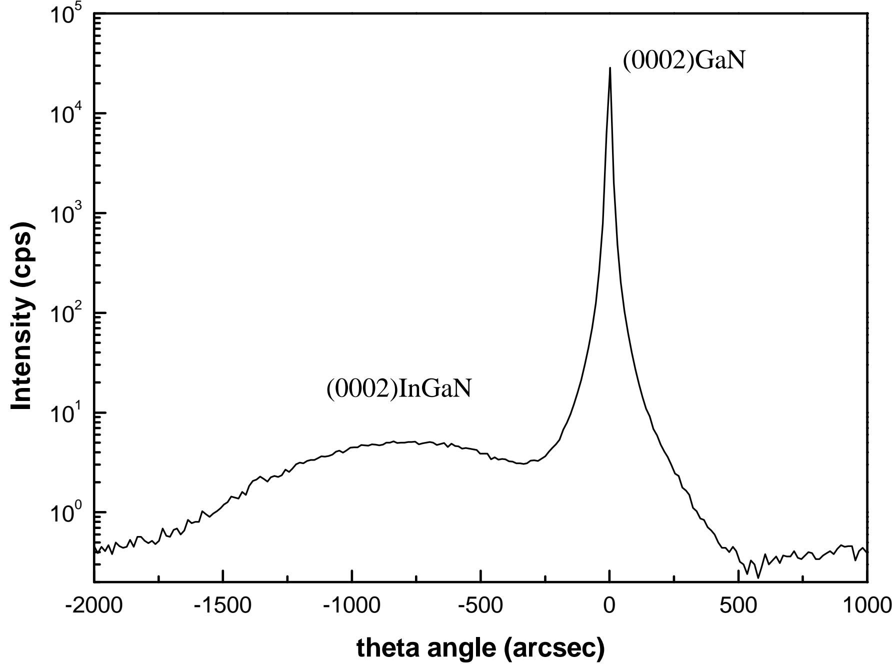

Figure 4.4: XRD theta-2theta scan of sample E3982.

$$\frac{\Delta c_o}{c_o} = -2\frac{c_{13}}{c_{33}}\frac{\Delta a_o}{a_o} \tag{4.1}$$

where

$$\begin{cases} \Delta c_o = c_{meas} - c_o & (4.2a) \\ \Delta a_o = a_{meas} - a_o & (4.2b) \end{cases}$$

where $a_o(x)$, $c_o(x)$ are the relaxed values of $In_xGa_{1-x}N$.

$$\frac{\Delta c_o}{c_0} = \frac{c_{meas} - [c_{GaN}(1-x) + xc_{InN}]}{c_{GaN}(1-x) + xc_{InN}} \tag{4.3}$$

$$\frac{\Delta a_o}{a_0} = \frac{a_{meas} - [a_{GaN}(1-x) + xa_{InN}]}{a_{GaN}(1-x) + xa_{InN}} \tag{4.4}$$

$$\frac{c_{13}(x)}{c_{33}(x)} = \frac{c_{13,GaN}(1-x) + xc_{13,InN}}{c_{33,GaN}(1-x) + xc_{33,InN}} \tag{4.5}$$

4.4 Design of Mesas

By using the same mask and following the same processing flow as in the first set of samples (Fig.3.6), the samples are patterned into various squared mesas 0.6μm height in order to expose laterally the InGaN layer for the PEC etching procedure. Fig.4.5 shows a schematic illustration of our mesas.

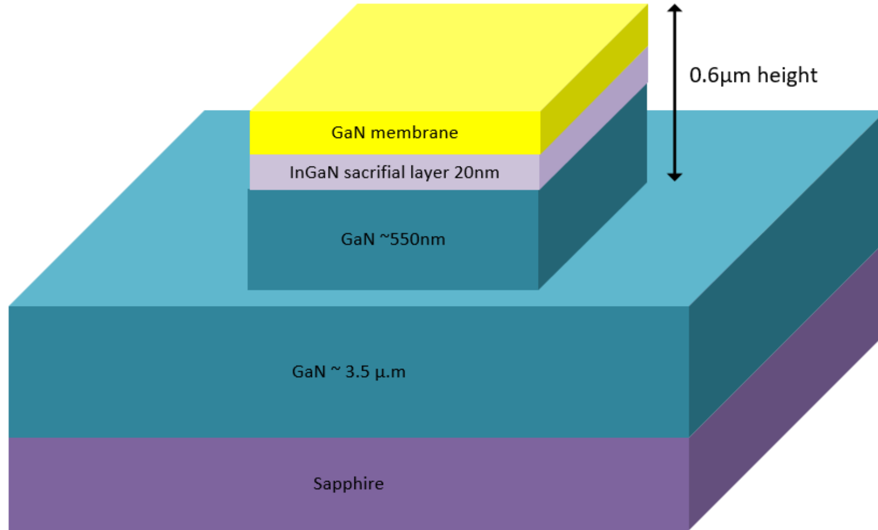

Figure 4.5: Schematic depicts the 1μm height squared mesas.

4.5 Photoelectrochemical Etching Procedure

After the modification of the as grown samples into mesas, we performed PEC etching experiments. Our initial excitation source was a CW laser diode at 405nm, considering that the nominal composition of InGaN sacrificial layer is $\sim$ 14%. Once more, our results were not satisfying as the InGaN layer did not seem to get etched. After XRD results came out, it was revealed that the indium composition was much less ($\sim$ 7.5%),

justifying the unsatisfactory results.

Taking into account that the PEC etching condition was not met with the 405nm laser diode as the estimated gap of InGaN based on the $\sim 7.4\%$ In-content is at $\sim 397nm$, we performed PEC etching using a tunable femtosecond pulsed laser varying the excitation wavelength from 380 to 400nm. We performed the same series of measurements on samples E3982 and E3934(first set of samples) where the top GaN membrane was 5nm-thick in both samples. Fig.4.7, 4.6 show the total, dark and photo-current as a function of time using the same PEC conditions, varying the light source wavelength from 380 to 400nm. Each subfigure in the two figures 4.6 and 4.7 correspond to a different spot on the sample, explaining the relative variation in the dark currents from one spot to another.

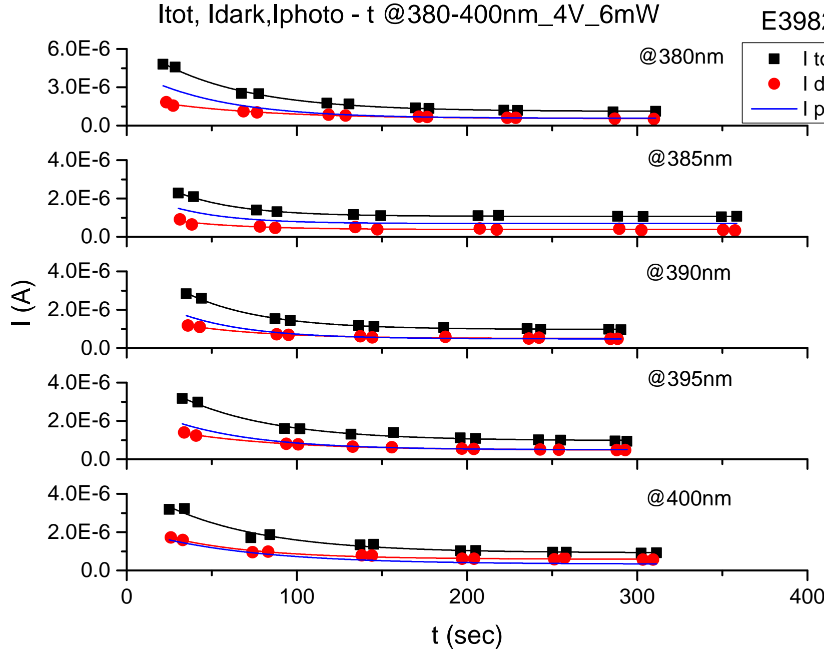

Figure 4.6: Diagrams show the total, dark and photo-current as a function of etching time with V=4Volts, P=6mW and $C = 4 \cdot 10^{-4} M$ for E3982.

The photo-current increases with respect to the decreasing wavelength of excitation as less and less carriers are absorbed. In our case, we have two different sacrificial layers in the two samples. In E3934 it is 5nm and in E3982 is 20nm. In general, the absorption probability is higher in the wider layer which, in our case, is E3982. However, as there is piezoelectric polarization due to different lattice constants in our heterostructures and

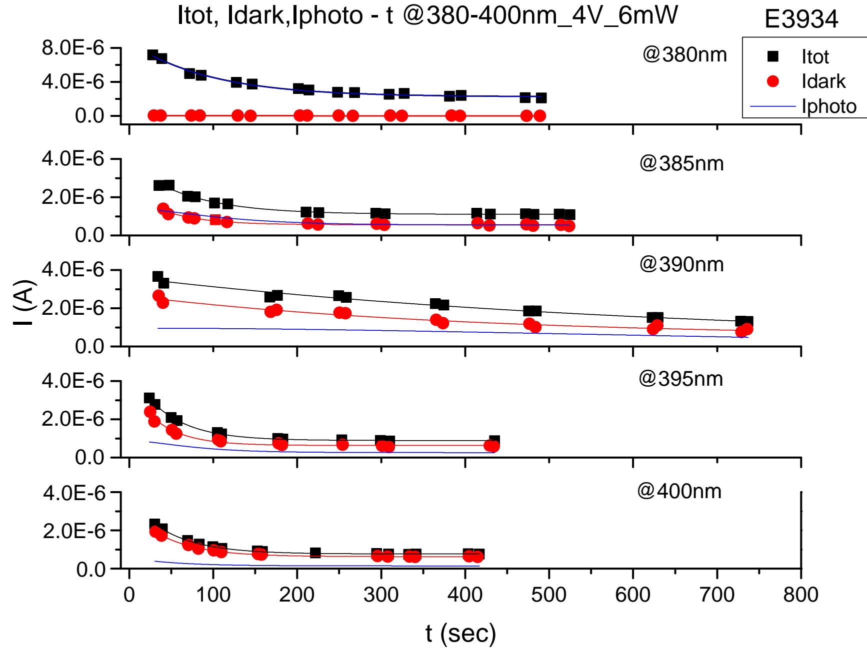

Figure 4.7: Diagrams show the total, dark and photo-current as a function of etching time with V=4Volts, P=6mW and $C = 4 \cdot 10^{-4} M$ for E3934.

to a lesser degree spontaneous polarization, this leads to quantum confined stark effect (QCSE). QCSE provokes band bending, leading the electrons to move to one side and the holes to the other. As a result, the wavefunction overlap between electron and holes in the wider 20nm QW is smaller than the 5nm QW. As a consequence, the absorption could be higher in E3934(5nm) than E3982(20nm) in this spectral range.

With decreasing wavelength of excitation the photo-current increases in both samples. This is more evident in Fig.4.8, where the spectral dependence of the photo-current in the two samples is shown. The tendency is stronger in sample E3934, where the photo-current is $< 1\mu A$ at 400nm and becomes more than $8\mu A$ at 380nm. The same but weaker tendency is observed in sample E3982, starting with a photo-current of about $2\mu A$ at 400nm and reaching a value of larger than $4\mu A$ at 380nm. The increase in photo-current with decreasing λ is attributed to increased absorption in the InGaN sacrificial layer, and the weaker wavelength dependence in sample E3982 can be explained by the larger InGaN layer thickness and the weakening effect of the QCSE in large QWs, making the absorption profile spectrally flatter.

In addition, by looking at graph 4.8, there are a couple of questions that arise:

1. In sample E3982 there is a non-negligible photo-current at 400nm. Could we use this photo-current for PEC etching?
2. In both samples, there is a significant photo-current at 380nm. Is this photo-current solely due to the InGaN layer or could we have some photo-current generation on other parts of the structure, as we approach the band-gap of the GaN buffer/substrate?

Another point of concern in Figures 4.6 and 4.7 is the large dark current values we observe in both samples, of the order of 1-2 μA in most spots.Moreover, the dark-current values decrease with etching-time, as if some kind of "curing" occurs on the diode surface. As a comparison, we note that in previous studies with 200nm-thick membranes the dark currents measured in PEC experiments were between $0.01 - 0.1\mu A$ and remained practically constant during the PEC experiment. We discuss again the dark current-issue in the next section.

Following the PEC etching experiments using different laser wavelengths, we observed each PEC spot with optical and SEM images, in order to assess the etching results. By using a 385nm laser diode, the mesas in the centre of the PEC spot appear differently coloured, possibly suggesting that the InGaN layer was etched, whereas by using a 390nm laser diode, the mesas show merely a dark grey colour (Fig. 4.9). In addition, the SEM images revealed that the GaN membranes on the top of our structures were more damaged with the 390nm light source whereas with 385nm they appeared more uniform (Fig.4.10). Moreover, there is a greyish shadow shown by arrows at the top-GaN/InGaN interface (less than 20nm depth) suggesting some initial etching of the InGaN layer. However, as GaN membrane is only 5nm thick, we are close to the limit of SEM resolution. In addition, we observe in Fig.4.11 an interface at $\sim 100nm$ depth, which is observed in almost all PEC experiments of the 2nd sample series. This interface is likely related to the beginning of MBE epitaxy on the GaN/Al_2O_3 template, which apparently exhibits some sensitivity to PEC etching conditions. Based on the above results, we selected the 385nm laser source as our excitation source.

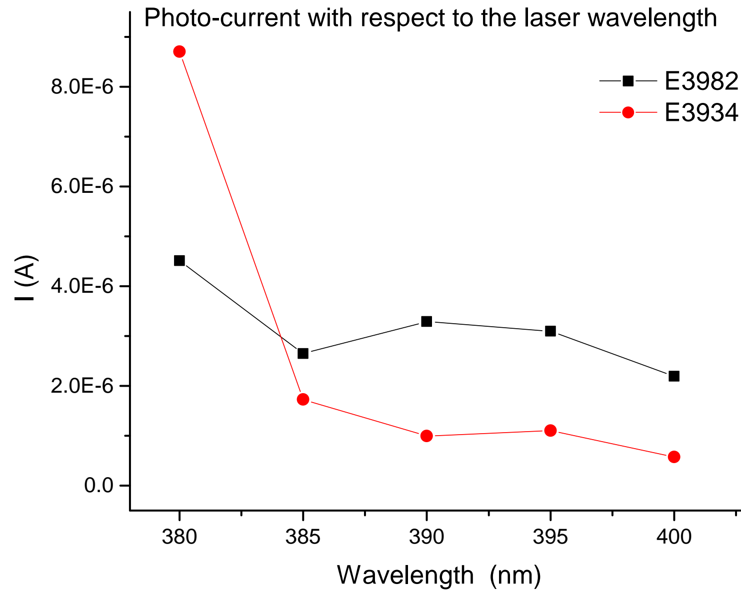

Figure 4.8: PEC: V=4Volts, P=6mW and $C = 4 \cdot 10^{-4} M$. Diagram presents the photo-current at t=0sec with respect to the laser wavelength, for samples E3934 and E3982.

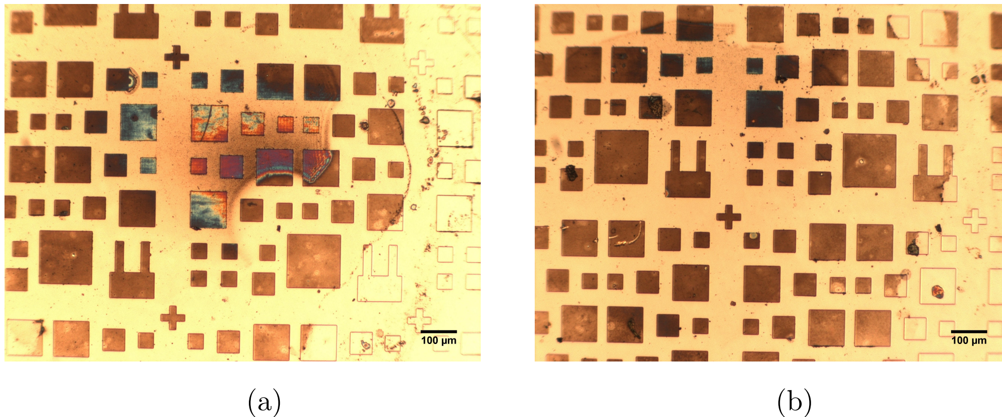

(a) (b)

Figure 4.9: PEC: V=4Volts, P≈6.00mW, $C = 4 \cdot 10^{-4} M$, t=2,400sec. Optical microscope images after PEC etching technique at (a) 385nm and (b) 390nm of sample E3982.

As a next step, in order to improve the etching results, we increased the duration of etching up to 3,600 secs by using the same voltage, power and concentration of KOH solution conditions. Fig.4.12 shows an optical image of the PEC spot, where there are slightly more mesas coloured. Moreover, there is a greyish shadow in the area between

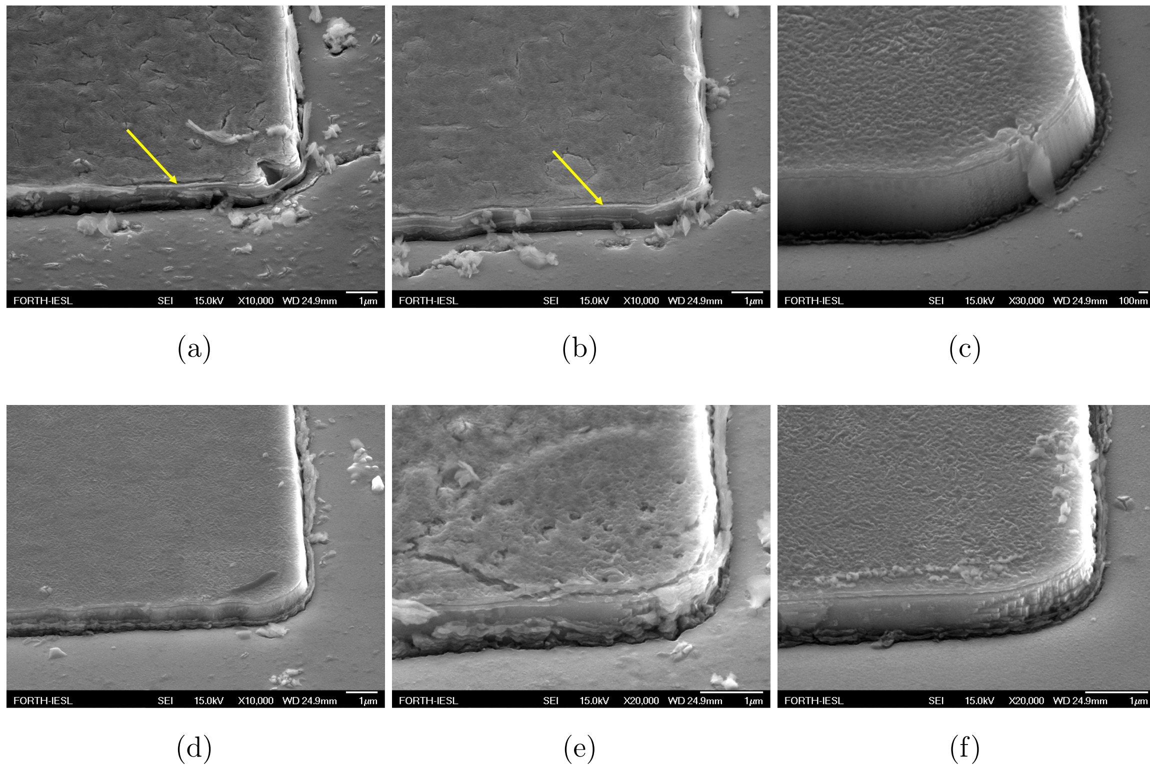

Figure 4.10: PEC: V=4Volts, P≈6.00mW, $C = 4 \cdot 10^{-4} M$, t=2,400sec. SEM images after PEC etching technique at (a)-(c) 385nm and (d)-(f) 390nm of sample E3982.

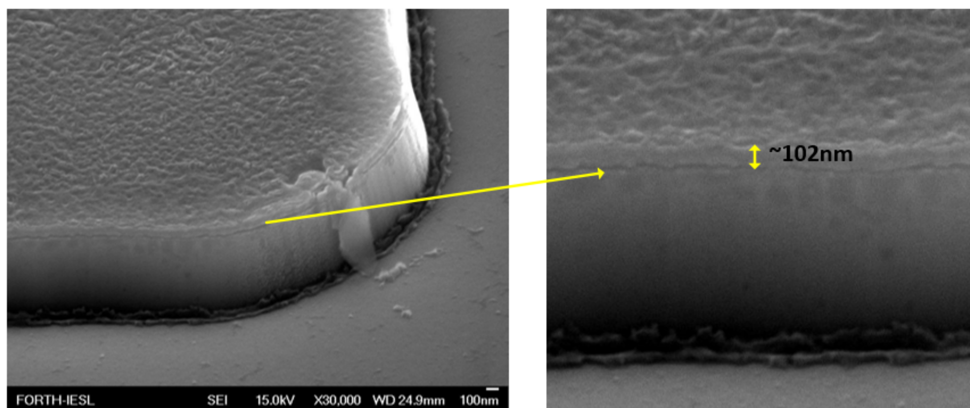

Figure 4.11: SEM image of a mesa of sample E3982 showing the interface at $\sim 102nm$ depth.

mesas indicating that the bottom GaN has been somehow affected. Furthermore, SEM images show some indications that GaN membranes have lifted up. However, there was no improvement on the mesas' surface.

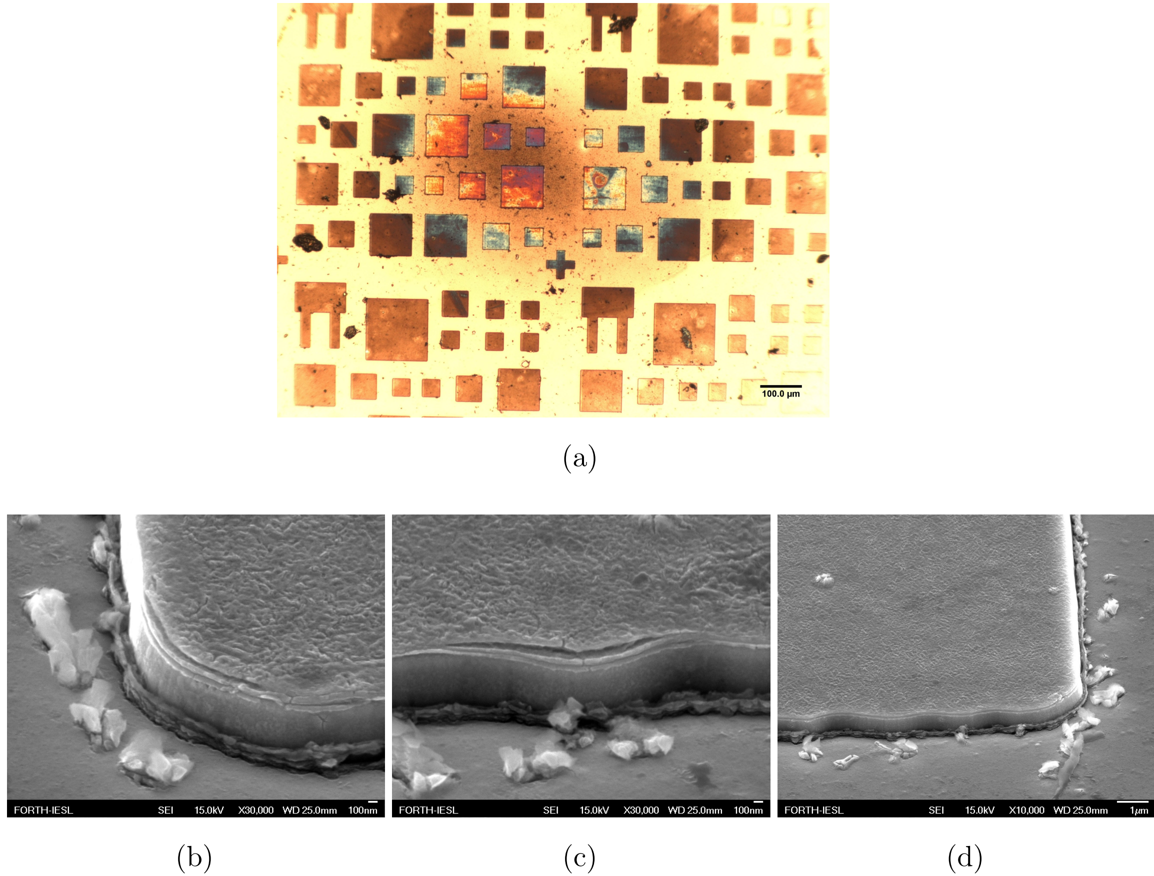

(a)

(b) (c) (d)

Figure 4.12: PEC: V=4Volts, P≈6.00mW, $C = 4 \cdot 10^{-4}M$, t=3,600sec. (a) An optical microscope image and (b)-(d) SEM images after PEC etching technique at 385nm of sample E3982.

In order to limit the damage of the membranes' surface, we performed several runs with varying powers of excitation while keeping all other etching parameters constant. Fig.4.13 presents the total, dark and photo-current as a function of etching time for 6mW, 3mW, 1.3mW and 0.770mW.

The main observation in Fig.4.13 is that the photo-current does not scale with power of excitation and remains practically constant, probably to some saturation effect. However, we observe differences in the colourization of mesas in these PEC experiments (Fig.4.12a,4.14). Decreasing the power from 6 to 3mW, more mesas in the centre of PEC spot have orange-blue colour. In addition, the greyish shadow between the mesas has weakened, suggesting that the GaN template is less affected. By decreasing further the excitation power, we see that the surface of mesas take a dark grey colour (Fig.4.14b,4.14c).

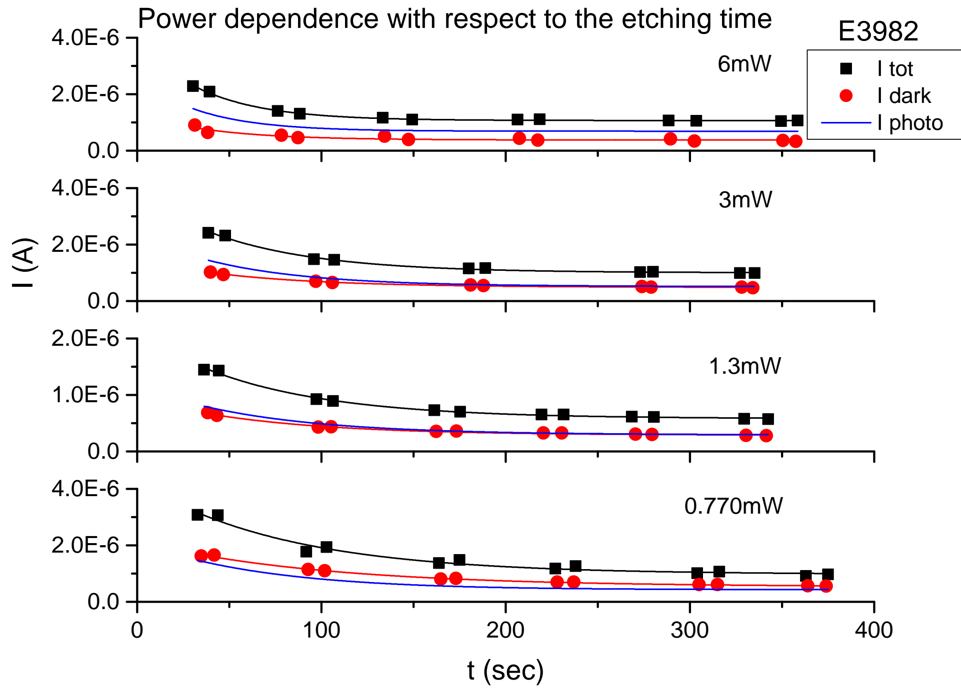

Figure 4.13: Diagram shows the total, dark and photo-current as a function of time of the sample E3982 with V=4Volts, $\lambda = 385nm$, t=3,600sec and $C = 4 \cdot 10^{-4}M$ for 6, 3 , 1.3 and 0.770 mW.

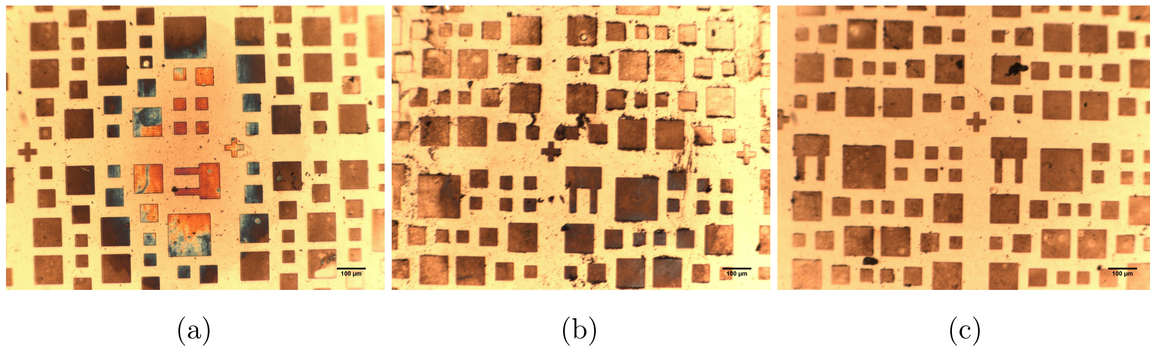

(a) (b) (c)

Figure 4.14: PEC: V=4Volts, $\lambda = 385nm$, $C = 4 \cdot 10^{-4}M$, t=3,600sec. Optical microscope images for (a) 3mW, (b)1.3mW and (c) 0.770mW after PEC etching technique of sample E3982.

By observing these PEC spots in SEM, we see no improvement on the mesas' surface, as the top GaN membranes seem damaged in all cases regardless of the excitation power of the laser source (Fig.4.15).

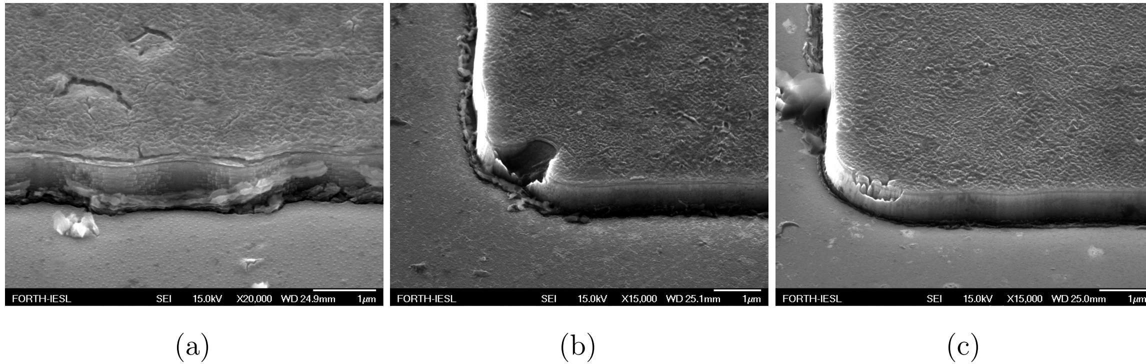

(a) (b) (c)

Figure 4.15: PEC: V=4Volts, $\lambda = 385nm$, $C = 4 \cdot 10^{-4}M$, t=3,600sec. SEM images for (a) 3mW, (b)1.3mW and (c) 0.770mW after PEC etching technique of sample E3982.

Summarizing the above, at first, we performed PEC etching by using a 405nm laser source as excitation power. Secondly, after XRD results revealed that the concentration of indium was $\sim$ 7.5%, we carried out experiments by using a fs-laser source between 380nm to 400nm. By assessing the etching results, we picked the 385nm laser wavelength as the most promising for the PEC etching procedure. Next, we tried to optimize the conditions of PEC for 385nm by increasing the time up to 3,600sec and by performing experiments at lower laser powers.

4.6 Transfer

After PEC etching procedure, we attempted to transfer the top-GaN membranes by using a PDMS stamp. PDMS was placed on the surface of every PEC spot and by removing it abruptly, we tried to lift up any free-standing GaN membrane. As a next step, we transferred the GaN pieces that were attached onto PDMS, to a Si/SiO_2 substrate. Fig.4.16 shows optical and SEM images of transferred pieces from sample E3982, where the top GaN membrane is 5nm thick, on SiO_2/Si. Fig.4.16a, 4.16b present some GaN membranes on the surface of Si/SiO_2 substrate, having a yellow colour arising from the reflection of the incident microscope light. After observing some of these pieces at SEM, we extracted their thickness to be $\sim 108nm$ after correcting for the angle of observation. This thickness corresponds well to the lateral etching occurring at $\sim 100nm$ beneath the top surface as commented in Fig.4.11. We believe that this interface appears due to

different epitaxial growth, as the GaN template is grown with Metal-Organic Chemical Vapor Deposition (MOCVD) whereas the rest of the samples is grown with MBE.

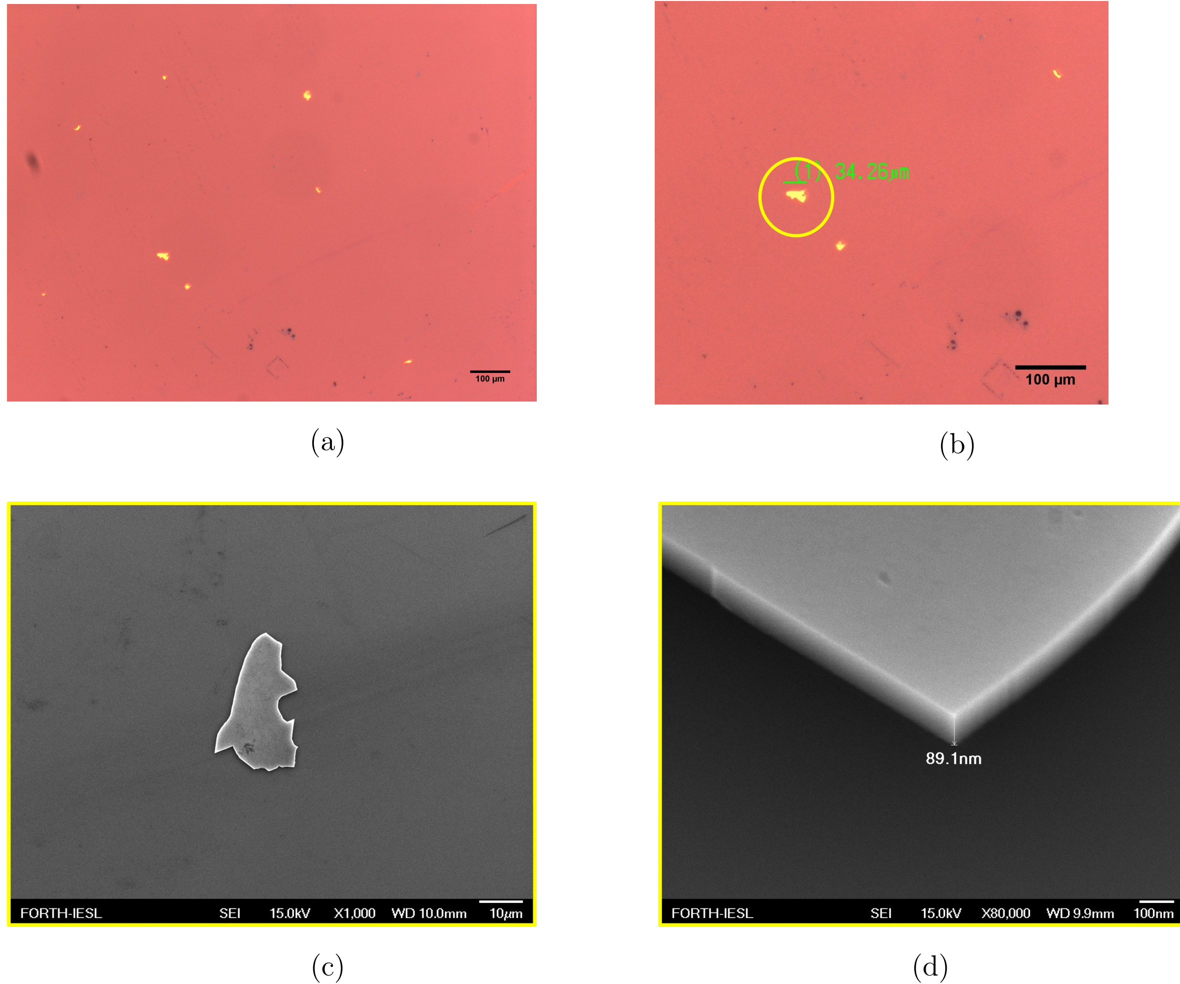

Figure 4.16: (a), (b) Optical images showing the transferred pieces of sample E3982. (c), (d) SEM images of the transferred fragment in yellow circle in optical image (b).

In these transfer experiments, we found no evidence of any 5nm-thick GaN membrane, either on the PDMS surface or after transferring the PDMS material onto the SiO_2/Si. This strongly suggests that in spite of the various colorizations observed in the PEC experiments, no "clean" lateral etching of the top GaN ultrathin layer has been achieved in our experiments. In order to comprehend this counter-result, we turned our attention to the dark-current characteristics of our diodes. Previous work on PEC etching of samples where the top-GaN membrane was 200nm-thick showed that the dark currents were much smaller $(0.01 - 0.1\mu A)$ than the photo-current and remained constant during

PEC etching. As an example, Fig.4.17 shows the variation of total current with PEC etching time. During the experiment, there have been "OFF" periods where the light beam is blocked. By observing the evolution of these "OFF" periods, we conclude that the initial dark current is much smaller than the respective photo-current and that the dark current remains constant throughout the PEC experiment [27].

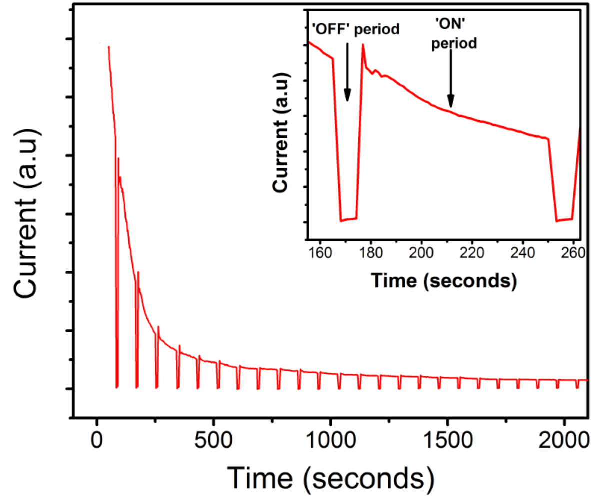

Figure 4.17: Variation of current with etching time under 4V dc bias in a sample with 200nm-thick top GaN. The inset shows a zoom-in on "ON-OFF" period.

In our samples, as dark current is decreasing with time during PEC etching (Fig.4.7, 4.6), we performed some dark electrochemical etching experiments in order to assess whether etching occurs also in the dark. Fig.4.18 shows the I-V measurements "before" and "after" dark etching procedure at V=4Volts, $C = 4 \cdot 10^{-4} M$, t=3,600sec of samples E3981 and E3983, where the top-GaN membrane is 30nm and 10nm thick respectively. It is evident that the dark current is decreasing significantly after dark-etching procedure indicating that some etching actually occurs. The I-V curves also suggest that there is big leakage current before dark experiments, whereas the diode seems to behave more like an ideal diode after that. The decrease of the dark current during the dark-etching runs is shown in 4.18b and 4.18d for the two samples.

The spots that have been subjected to dark-etching experiments are subsequently studied in SEM. We observe that the top-surface of sample E3983 with a 10nm-thick GaN on top shows clear signs of vertical etching (see arrows), whereas in sample E3981 with the 30nm-thick GaN there are no signs of vertical etching. This difference seems to suggest

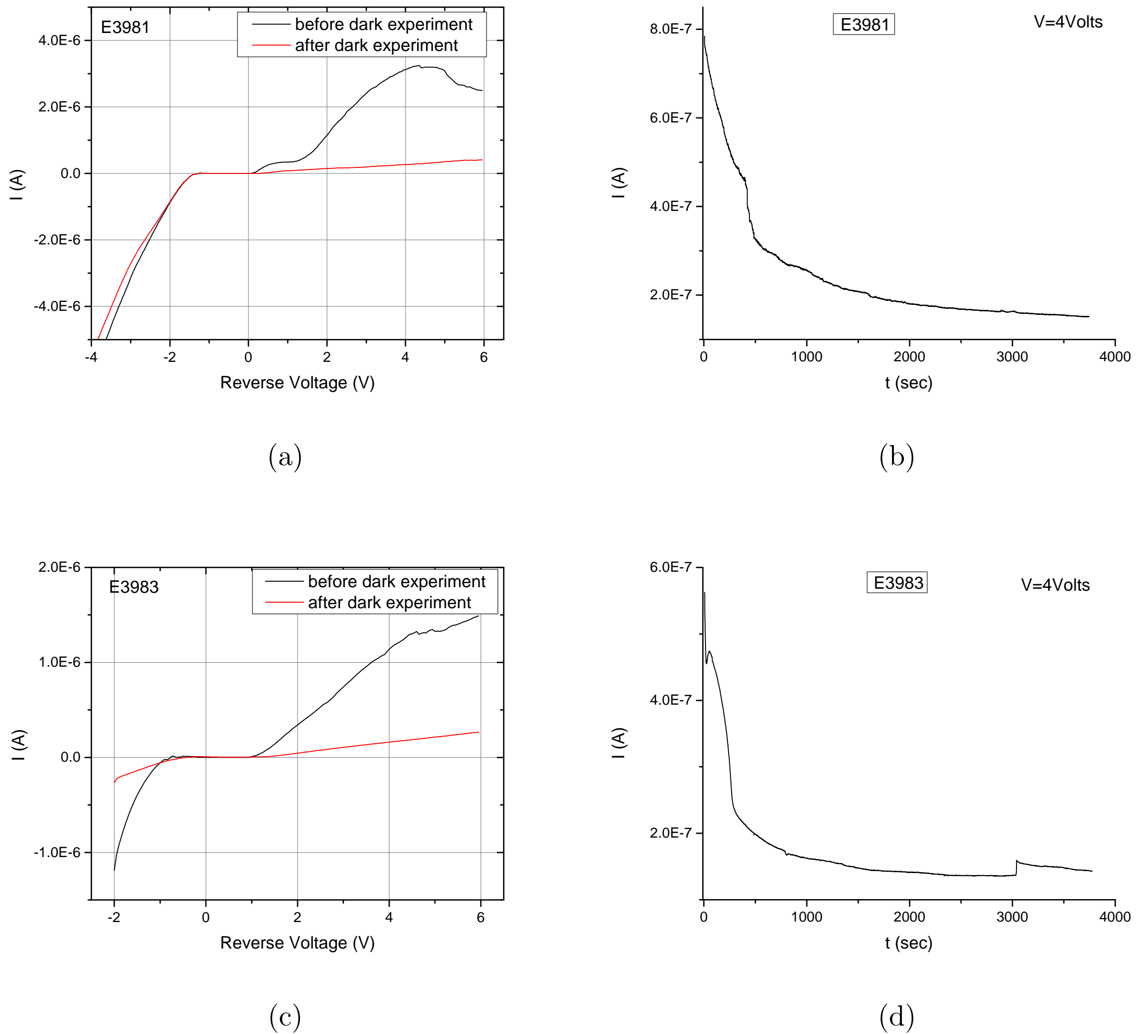

Figure 4.18: Plots show (a), (c) the I-V measurements before and after dark electrochemical experiments and (b), (d) the dark current as a function of etching time under 4V reverse bias of sample E3981 and E3983.

that at least part of the dark current involves carrier transport from the electrolyte to the semiconductor mesas' surface via the top GaN layer, which somehow is associated with some vertical etching. Obviously, this component of the dark current is expected to be larger in the 10nm-GaN sample, as for these small thicknesses carrier tunneling is quite probable. Another observation in Fig.4.19 is the absence of lateral etching at the MBE/MOCVD interface 100nm beneath the surface. We conclude then, that this lateral etching occurs only under illumination.

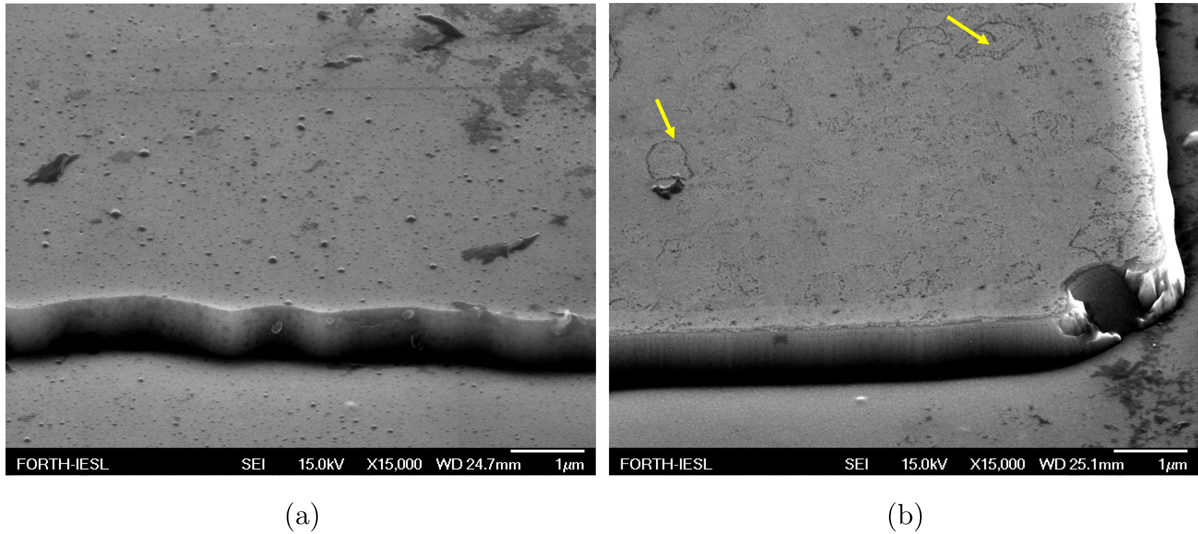

(a) (b)

Figure 4.19: SEM images show the surface of mesas after dark experiments at 4V reversed bias of (a) E3981 and (b) E3983 sample.

Moreover, we performed another dark-etching experiment at V=1Volt on sample E3983 (10nm thick GaN-membrane). From the I-V plot (Fig.4.18c), we see that the dark-current at 1V is low enough ($\sim nA$) and we would like to test whether there will be any damage on the membrane. After dark etching for about 1 hour, we observed the spot area at SEM. Fig.4.20 presents that both the surface of mesas and the area between mesas show clear signs of damage, in spite of the very low dark current in these experiments (Fig.4.21).

Finally, we performed PEC etching on sample E3981 (30nm-thick GaN membrane) by using an excitation source at $\lambda = 385nm$ based on previous work on sample E3982. Fig.4.22 shows the optical and SEM images of this spot area. In the optical image (Fig.4.22a), we observe that the mesas have a dark grey-blue colour indicating that their surface is damaged (as previous PEC spots in Fig.3.13 have shown). This is more evident by SEM images, where the top-GaN membrane seems to be attacked vertically. As a consequence, it is clear that the PEC etching technique does not work with these samples. Due to the low In-composition, the excitation source used in our experiments is too close to the GaN gap resulting in some direct photo-etching of the GaN surface. In order to improve the etching results, we must have an increase of the indium composition in the InGaN sacrificial layer for the purposes of selective etching.

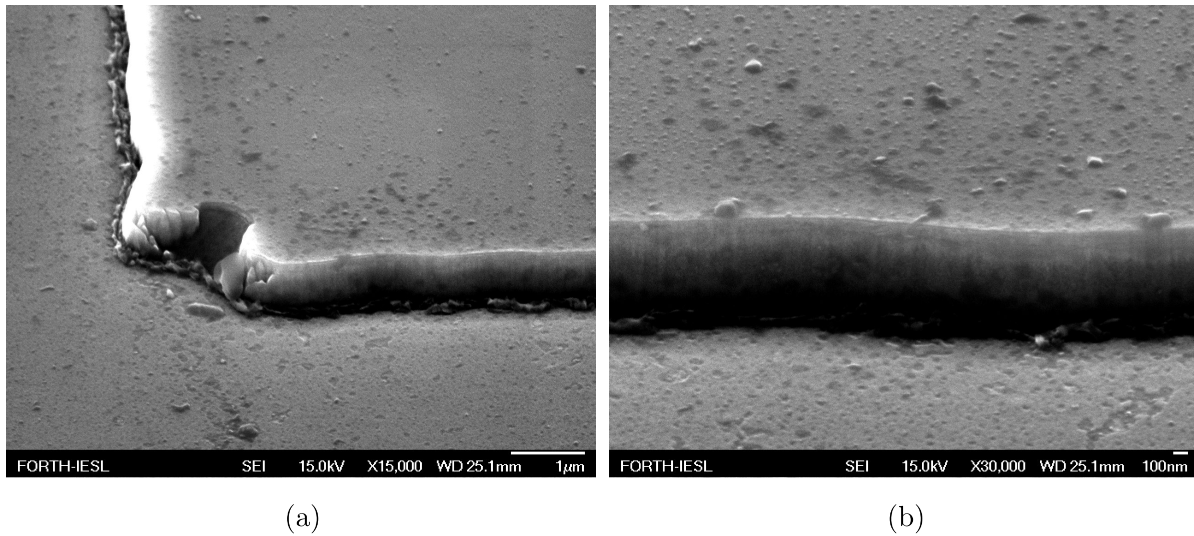

(a) (b)

Figure 4.20: SEM images show the surface of mesas after dark experiments at 1V reversed bias of E3983 sample.

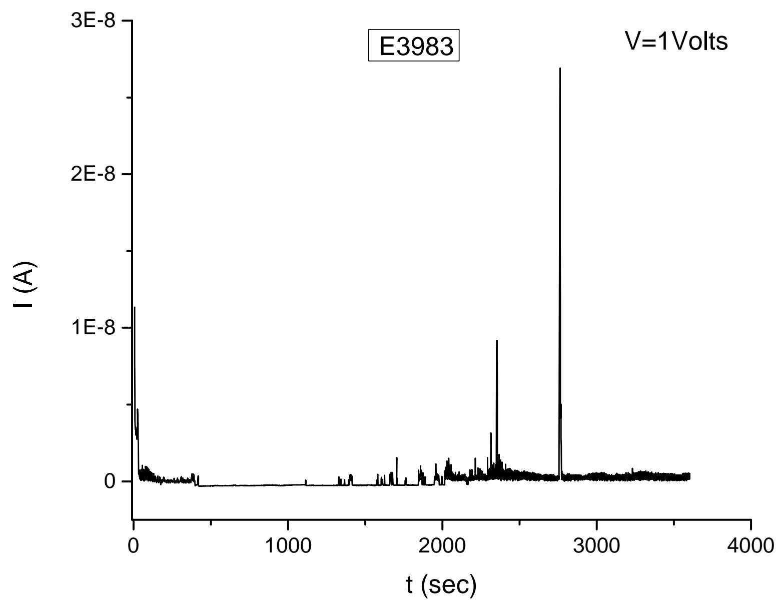

Figure 4.21: The variation of dark current under 1V reversed bias of sample E3983.

To summarize this section, we tried to transfer the GaN-membranes of different thicknesses by using a PDMS stamp. As we did not manage to achieve smooth lateral etching of the GaN membrane, we did not succeed in transferring them on the Si/SiO_2

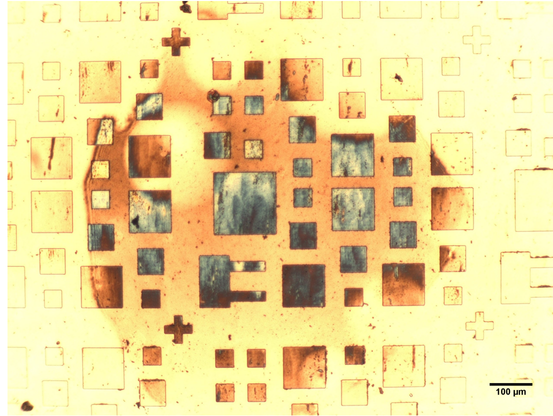

(a)

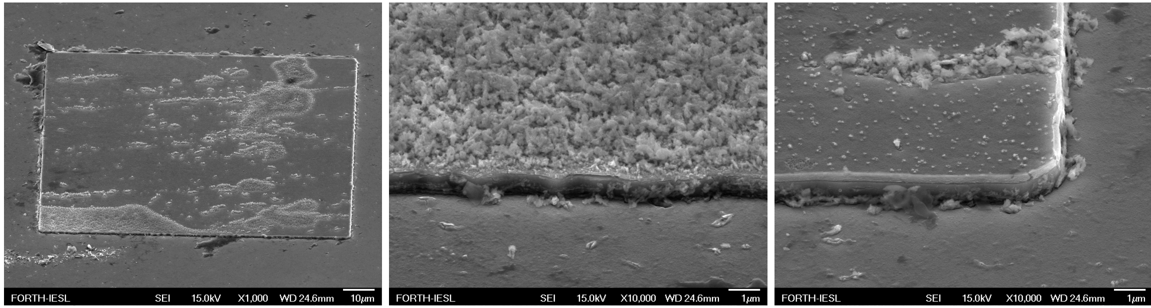

(b) (c) (d)

Figure 4.22: PEC: V=4Volts, P≈6.00mW, $C = 4 \cdot 10^{-4}M$, t=2,400sec. (a) An optical microscope image and (b)-(d) SEM images after PEC etching technique at 385nm of sample E3982.

substrate. However,we transferred 100nm-thick membranes due to some lateral etching occurring at the MBE/MOCVD interface. This etching is photo-activated. Moreover, we performed dark I-V measurements and dark-etching experiments to understand the decreasing dark current during PEC etching. We saw that the surface of mesas following dark-etching is etched for sample E3983 with 10nm-thick GaN membrane whereas for sample E3981 it did not seem to be affected. As a consequence, we performed dark-etching at 1V for sample E3983 in order to limit the dark current effect on the surface of mesas. The results were not satisfying as the GaN membrane was damaged once more. We believe that the thickness (10nm) of the top-GaN membrane is critical for PEC etching technique as other processes, such as tunneling, may cause vertical etching of surface. Moreover, we performed PEC etching on sample E3981 by using an excitation source

at $\lambda = 385nm$. The surface of top-GaN membrane was etched, as optical microscope and SEM images showed. In all the above discussion, we believe that the PEC etching technique does not work properly in structures where the top-GaN membrane is thin enough for some other processes to be favoured. In order to improve the PEC technique, we believe that the surface of our mesas should be protected by depositing a few layers of HfO_2. In addition, we suppose that the indium composition ($\sim 7.5\%$) played an important role for the unsatisfying results. The excitation source had to become close enough to the GaN gap and as a result the GaN surface of mesas was vertically etched.

4.7 Conclusions

In this chapter, we described the experiments performed on the second set of samples E3981-83. Their design was the outcome of previous work on the first set of samples E3933-35, as we assumed that the AlGaN layer increased the roughness of top-GaN membranes, as well as affected the homogeneity of indium composition in the InGaN sacrificial layer. Firstly, we characterized the as-grown samples with AFM, PL and XRD measurements. AFM showed that the surface of GaN membranes has been improved in comparison with the roughness values on the first set of samples. In addition, XRD provided information about the lower-than-nominal composition of InGaN layer, which played a major role in PEC experiments that followed. Furthermore, we performed PEC experiments with different laser sources in order to pick the best excitation source for our structures based on the etching results. In addition, by using a laser diode at $\lambda = 385nm$, we tried to improve the etching results by using different excitation powers and by changing the duration of PEC etching. After PEC procedure, we tried to transfer the GaN membranes on a Si/SiO_2 substrate by using PDMS. We did not succeed to transfer any piece of thin GaN membrane as PEC technique did not work out. Moreover, we performed some dark-etching experiments in order to understand the decreasing behavior of dark current during PEC. As a result of these experiments, we saw that the surface of mesas where the GaN membrane was 10nm-thick was attacked even in the dark, suggesting that its thickness is critical for PEC technique, and that other mechanisms take place and participate in the vertical etching of GaN. On the other hand, the 30nm-thick GaN membranes of sample E3981 were not affected by dark etching. In addition, PEC experiments on this sample

showed an etched GaN surface. We suppose that the indium composition is low enough and as a consequence the laser wavelength that we used for our experiments excited deep levels of GaN, enabling their participation to PEC etching procedure.

On the basis of estimates of future perspectives of PEC etching technique on III-nitrides heterostructures for the fabrication of ultra-thin GaN membranes, we believe that the indium consistency in the InGaN sacrificial layer should be risen to $\sim 14\%$. In this way, the spectral range emission of InGaN layer will not overlap with GaN's gap and the selectivity of PEC etching technique will be re-instored. Moreover, as far as the surface of mesas is concerned, we assume that their etching can be avoided by their protection with a few layers of HfO_2. This approach will eliminate vertical etching of GaN membrane, which is not desirable, and only lateral etching of InGaN sacrificial layer will be able to occur.

Bibliography

[1] *Electric Field Effect in Atomically Thin Carbon Films | Science*. URL: https://science.sciencemag.org/content/306/5696/666.

[2] *Transport through graphene quantum dots - IOPscience*. URL: https://iopscience.iop.org/article/10.1088/0034-4885/75/12/126502/meta.

[3] *Rev. Mod. Phys. 81, 109 (2009) - The electronic properties of graphene*. URL: https://journals.aps.org/rmp/abstract/10.1103/RevModPhys.81.109.

[4] *Two-dimensional non-layered materials - ScienceDirect*. URL: https://www.sciencedirect.com/science/article/pii/S2588842019301208.

[5] *2D Materials: An Introduction to Two-Dimensional Materials | Ossila*. URL: https://www.ossila.com/pages/introduction-2d-materials.

[6] *Wurtzite crystal structure*. In: *Wikipedia*. Page Version ID: 891305951. Apr. 7, 2019. URL: https://en.wikipedia.org/w/index.php?title=Wurtzite_crystal_structure&oldid=891305951.

[7] *GaN, AlN, and InN: A review: Journal of Vacuum Science & Technology B: Microelectronics and Nanometer Structures Processing, Measurement, and Phenomena: Vol 10, No 4*. URL: https://avs.scitation.org/doi/abs/10.1116/1.585897.

[8] *Two dimensional electron gases induced by spontaneous and piezoelectric polarization in undoped and doped AlGaN/GaN heterostructures: Journal of Applied Physics: Vol 87, No 1*. URL: https://aip.scitation.org/doi/10.1063/1.371866.

[9] *Spontaneous and piezoelectric polarization effects in III–V nitride heterostructures: Journal of Vacuum Science & Technology B: Microelectronics and Nanometer Structures Processing, Measurement, and Phenomena: Vol 17, No 4*. URL: https://avs.scitation.org/doi/abs/10.1116/1.590818.

[10] Bo-Ting Liou, Sheng-Horng Yen, and Yen-Kuang Kuo. "Vegard's law deviation in band gaps and bowing parameters of the wurtzite III-nitride ternary alloys". In: Photonics Asia 2004. Ed. by Jian-quan Yao, Yung Jui Chen, and Seok Lee. Beijing, China, Jan. 20, 2005, p. 296. DOI: 10.1117/12.575300. URL: http://proceedings.spiedigitallibrary.org/proceeding.aspx?doi=10.1117/12.575300.

[11] Zakaria Y. Al Balushi et al. "Two-dimensional gallium nitride realized via graphene encapsulation". In: *Nature Materials* 15.11 (Nov. 2016), pp. 1166–1171. ISSN: 1476-1122, 1476-4660. DOI: 10.1038/nmat4742. URL: http://www.nature.com/articles/nmat4742.

[12] Yunxu Chen et al. "Growth of 2D GaN Single Crystals on Liquid Metals". In: *Journal of the American Chemical Society* 140.48 (Dec. 5, 2018), pp. 16392–16395. ISSN: 0002-7863. DOI: 10.1021/jacs.8b08351. URL: https://doi.org/10.1021/jacs.8b08351.

[13] M. S. Minsky, M. White, and E. L. Hu. "Room-temperature photoenhanced wet etching of GaN". In: *Applied Physics Letters* 68.11 (Mar. 11, 1996). Publisher: American Institute of Physics, pp. 1531–1533. ISSN: 0003-6951. DOI: 10.1063/1.115689. URL: https://aip.scitation.org/doi/abs/10.1063/1.115689.

[14] *X-ray crystallography - Wikipedia*. URL: https://en.wikipedia.org/wiki/X-ray_crystallography.

[15] W.Callister and D.Rethwisch. *Fundamentals of Materials Science and Engineering*. 4th edition. J.Wiley and Sons Inc, 2013. Chap. 3. ISBN: 9781118324578.

[16] *Miller index - Wikipedia*. URL: https://en.wikipedia.org/wiki/Miller_index.

[17] *Scanning Electron Microscopy (SEM) and Transmission Electron Microscopy (TEM) for Materials Characterization*. URL: https://www.researchgate.net/publication/305446136_Scanning_Electron_Microscopy_SEM_and_Transmission_Electron_Microscopy_TEM_for_Materials_Characterization.

[18] *Scanning electron microscope - Wikipedia*. URL: https://en.wikipedia.org/wiki/Scanning_electron_microscope.

[19] *Scanning electron microscopy*. URL: https://www.slideshare.net/JessaArio/scanning-electron-microscopy.

[20] *Photoluminescence - Wikipedia*. URL: https://en.wikipedia.org/wiki/Photoluminescence.

[21] *Atomic force microscopy - Wikipedia*. URL: https://en.wikipedia.org/wiki/Atomic_force_microscopy.

[22] *Atomic Force Microscope Principle | AFM Scanning | How AFM Works*. URL: https://parksystems.com/medias/nano-academy/how-afm-works.

[23] *Polydimethylsiloxane*. In: *Wikipedia*. Page Version ID: 959856422. URL: https://en.wikipedia.org/w/index.php?title=Polydimethylsiloxane&oldid=959856422.

[24] *Introduction to poly-di-methyl-siloxane (PDMS)*. Elveflow. Library Catalog: www.elveflow.com. URL: https://www.elveflow.com/microfluidic-reviews/general-microfluidics/the-poly-di-methyl-siloxane-pdms-and-microfluidics-2/.

[25] Andres Castellanos-Gomez et al. "Deterministic transfer of two-dimensional materials by all-dry viscoelastic stamping". In: *2D Materials* 1.1 (). Publisher: IOP Publishing, p. 011002. ISSN: 2053-1583. DOI: 10.1088/2053-1583/1/1/011002. URL: https://doi.org/10.1088%2F2053-1583%2F1%2F1%2F011002.

[26] X. Y. Liu and T. G. Andersson. "Surface roughness of GaN and thin AlGaN layers grown by molecular beam epitaxy". In: *Applied Surface Science* 226.4 (Mar. 30, 2004), pp. 331–334. ISSN: 0169-4332. DOI: 10.1016/j.apsusc.2003.10.043. URL: http://www.sciencedirect.com/science/article/pii/S0169433203012285.

[27] *Thesis: Novel approaches for robust polaritonics - ID: 38971*. URL: http://thesis.ekt.gr/thesisBookReader/id/38971#page/82/mode/2up.